Input-Output Properties of the Power System Swing Dynamics: Identification, Model Reduction, and Controller Design

Final Project Report

S-79G

Power Systems Engineering Research Center
Empowering Minds to Engineer
the Future Electric Energy System

Input-Output Properties of the Power System Swing Dynamics: Identification, Model Reduction, and Controller Designs

Final Project Report

Project Team

Sandip Roy, Project Leader

Vaithianathan (Mani) Venkatasubramanian

Washington State University

Graduate Students

Mohammadreza Hatami

Kasra Koorehdavoudi

Washington State University

PSERC Publication 21-05

March 2021

For information about this project, contact:

Sandip Roy
Professor, School of Electrical Engineering and Computer Science
Washington State University
Email: sandip@wsu.edu

Power Systems Engineering Research Center

The Power Systems Engineering Research Center (PSERC) is a multi-university Center conducting research on challenges facing the electric power industry and educating the next generation of power engineers. More information about PSERC can be found at the Center's website: http://www.pserc.org.

For additional information, contact:

Power Systems Engineering Research Center
Arizona State University
527 Engineering Research Center
Tempe, Arizona 85287-5706
Phone: 480-965-1643
Fax: 480-727-2052

Notice Concerning Copyright Material

PSERC members are given permission to copy without fee all or part of this publication for internal use if appropriate attribution is given to this document as the source material. This report is available for downloading from the PSERC website.

© 2021 Washington State University. All rights reserved.

Acknowledgements

We wish to thank the industry advisors for the project, Patrick Panciatici, Florent Xavier, and Thibault Prevost, for their support and advice throughout the project.

Executive Summary

Changing operational paradigms, including increasing penetration of intermittent renewables, growing use of demand-side power management, and higher sophistication of distributed systems (e.g. increased reliance on distributed generation), are introducing uncertainty and variability in the operating point of the bulk power grid. This variability and uncertainty in grid operations potentially makes the system susceptible to undesirable dynamics, including sustained or poorly-damped natural oscillations, wide-area propagative responses to impulsive disturbances, forced oscillations, etc. These oscillations and propagative responses, if not properly managed, can incur cascading failures and cause outages at the regional or even continental scale. Indeed, numerous instances of such wide-area dynamic responses have been recorded during the last few years, and some have led to significant outages. Prevention and mitigation of such wide-area dynamic responses critically requires deployment, tuning, and coordination of appropriate control systems. New technologies, including new sensing modalities and power electronics, are enabling new controls which together with legacy systems can be used to manage oscillations and disturbances. However, the increased variability and uncertainty in grid operations is also making the design and coordination of control systems more challenging.

Motivated by the need for and challenges inherent to the control of dynamic oscillations and disturbances, here we undertake a study of control channels and control system coordination for the bulk power grid's swing dynamics. Traditionally, the analysis of swing dynamics has been centered around characterizing the modal responses of the system. In an earlier PSERC project, we pursued a study of input-output channels for the classical model of the swing dynamics. Our initial effort established that input-output channels can exhibit properties such as nonminimum-phase zeros which complicate control and alter disturbance responses, and also identified some structural properties of the power networks that can result in nonminimum-phase dynamics.

Relative to our earlier study, the research undertaken in this project had three main aims. First, a more comprehensive structural assessment of channel properties was undertaken for the swing-dynamics model. Second, we studied the influence of deployed controllers on the internal (modal) characteristics of the swing dynamics, as well as the input-output properties of a second remote control channel. in this effort, we focused primarily on understanding how HVDC modulation would impact properties of a remote control; this study was primarily motivated by the deployment of HVDC modulation on the France-Spain interchange, and the concern that this control may interact with other nearby generator controls in the European grid. Third, we undertook a study of input-output properties in more sophisticated models of the swing dynamics, which more realistically represent the dynamics of intertial generators. In undertaking these studies, we also characterized control-channel properties and simulated channel behaviors in a small swing-dynamics model deriving from a planning scenario for off-shore wind farms in the French power grid.

The main findings of our study are as follows:

1) The presence or absence of nonminimum-phase zeros for an input-output channel play a crucial role in determining the behavior of the system when a control is implemented on that channel, or a disturbance occurs. The presence of nonminimum-phase zeros depends in a complicated way on the multi-path structure of the power network, as well as the

parameters of lines and generators in the network (including inertias, dampings, etc). We have developed both qualitative and numerical characterizations of the zeros in terms of these parameters.

2) HVDC modulation can alter input-output properties of remote channels, and hence may interact with other control systems in complicated ways. We have modeled HVDC modulation within the classical swing-dynamics model, and characterized its impact on the zeros of both collocated and remote channels. Importantly, HVDC modulation often improves the input-output characteristics of channels, but may in special cases introduce nonminimum-phase behaviors in remote channels.

3) Channel properties have been studied for more sophisticated models of the swing dynamics, which more fully represent the states of inertial generators, using numerical examples. These studies show that many channel properties established for the classical model carry through to the more detailed models, but these models may also exhibit unexpected non-minimum-phase behaviors arising due to the additional generator dynamics.

4) The characterization of zero structure and channel interactions in models for the swing dynamics is a promising starting point for developing model-reduction algorithms which maintain input-output properties, and hence are predictive of control responses.

As a whole, our study clarifies the complexity inherent to wide-area control of swing dynamics in today's highly variable power grid, and the possibility for undesirable interactions among multiple control systems. Our study also provides a set of guidelines for understanding the properties of control channels and interactions among controllers, which we hope will be a starting point toward effective algorithms for coordination of controls in the grid.

The research developed in this project is partially described in the following publications and reports.

Project Publications:

[1] Koorehdavoudi, Kasra, Sandip Roy, Thibault Prevost, Florent Xavier, Patrick Panciatici, and Vaithianathan Mani Venkatasubramanian. "Input-output properties of the swing dynamics for power transmission networks with hvdc modulation." *IFAC-PapersOnLine* 50, no. 1 (2017): 5442-5447.

[2] M. Hatami, V. Venkatasubramanian, S. Roy, P. Panciatici, T. Prevost, F. Xavier, ``Study of Non-minimum Phase Zeros in Test Power Systems from Wide-Area Control Designs," in 2017 IREP Symposium, Porto, Portugal, August 2017.

[3] Koorehdavoudi, Kasra, Sandip Roy, Jackeline Abad Torres, and Mengran Xue. "Interactions among control channels in dynamical networks." In 2017 IEEE 56th Annual Conference on Decision and Control (CDC), pp. 1058-1063. IEEE, 2017.

[4] Koorehdavoudi, Kasra, Sandip Roy, Jackeline Abad Torres, and Mengran Xue. "Impacts of high and low gain controllers on remote channels in dynamical networks." In 2018 IEEE Conference on Decision and Control (CDC), pp. 3680-3685. IEEE, 2018.

Table of Contents

List of Figures

List of Tables

1. Introduction

1.1 Background

The growing stress on and variability of the bulk power grid are motivating the development of new control systems for damping wide-area oscillations. At the same time, new technologies -- including synchrophasors, new power electronics, and pervasive communications – are enabling the deployment of heterogeneous new feedback controls. In consequence, the bulk grid is evolving toward a ``controls-rich" system, which has a wide array of control systems capable of influencing the grid swing dynamics. Wide-area control capabilities that are being deployed more frequently in the grid include HVDC modulation and various Flexible AC Transmission (FACTS) controllers, among others.

1.2 Overview of the Problem

New control capabilities being deployed in the power grid have the potential for improving its dynamics, by increasing efficiency while also reducing the frequency of disruptions. However, appropriate design and operation of grid controls is challenging for several reasons. First, as the penetration of intermittent renewables and distributed generation increases, the operating profile of the grid (including generation, load, congestion, and inertia patterns) is becoming increasingly variable. In consequence, the impacts of new controls on the swing dynamics must be evaluated across the wide range of possible operating conditions, which may be computationally extremely taxing given the complexity of large-scale dynamic simulations. This computational challenge is further amplified when controller design is required, since simulations must also be performed over the design space. Second, the design and management of grid controls increasingly requires understanding and shaping interactions among multiple control system, as heterogeneous new controls are deployed; managing such control-system interactions is further complicated by the fact that different authorities may be responsible for the operation and tuning of the various control systems. Third, the management of grid controls is challenging because of the difficulty in gaining real-time situational awareness of grid dynamics under ambient operational conditions.

While there is an extensive literature regarding the swing dynamics of the bulk power grid [1], these studies do not directly address the challenges listed above, so as to enable systematic analysis and design of controls. One main reason is that formal analysis has almost entirely focused on the *modes* of the linearized swing dynamics, which only give insight into the internal properties of the dynamics. Control-system analysis and design require characterizing input-output properties of the dynamics, and so require a full input-output or transfer-function analysis rather than only a modal viewpoint. Specifically, a transfer-function analysis is needed for evaluating the putative impacts of planned controls, and thus guiding their design.

1.2.1 Main Issues

Assessing new control systems deployed in the bulk grid to damp oscillations requires investigating the following main issues:

1) Structural and topological characterization of input-output channels or transfer functions in the classical model for the swing dynamics.
2) Analysis of control channel interactions in the classical model. That is, the impact of one deployed control (e.g. HVDC modulation) on a second control channel needs to be characterized.
3) Assessment of input-output channels, and channel interactions, for more sophisticated models for the swing dynamics.

1.2.2 Secondary Issues

To address the primary issues revolving around assessment of controls for swing dynamics in the bulk power grid, some secondary issues regarding modeling of grid dynamics and controls also need to be addressed. One particular need is to appropriately represent emerging grid controls within the scope of network models for the swing dynamics. In this study, we focused particularly on representing HVDC modulation within models for the swing dynamics. While HVDC lines have been extensively deployed, modulation has only been used in very limited circumstances, and hence their impacts on the swing dynamics have not been fully modeled. In the scope of our effort, we propose such models. We also tangentially discuss models for other power-electronics-enabled controls, but do not develop such models in detail.

1.3 Report Organization

The report is organized in two sections. The analysis of control channels and control interactions in the classical model for the swing dynamics is presented in Section 2. Simulation-based analyses of control channels for more sophisticated models of the swing dynamics are described in Section 3.

2. Assessing HVDC Modulation Impacts on Remote Grid Channels

2.1 Scope and Motivation

The bulk power transmission network is being subject to increasing stress and uncertainty due to renewables integration, changing regulatory paradigms, and use of new devices and technologies (e.g., power electronics, syncrophasors), among other reasons [2-5]. This increased stress and variability is complicating the analysis and control of transients/oscillations in the grid, and necessitating network-theoretic analysis of disruptions as well as wide-area control strategies. Analyzing disruptions and designing wide-area controls, at its essence, requires understanding input-output properties of the power network's swing dynamics. There is a particular interest in developing structural and graph-theoretic insights into the input-output dynamics, as a stepping stone toward practical analysis and control design. In previous work, we developed structural and graph-theoretic results into the zeros of input-output channels for the classical swing dynamics model [6], so in this article we expand this analysis framework to encompass networks with controlled high-voltage direct-current (HVDC) lines.

The analysis of input-output dynamics developed here informs, particularly, the deployment and design of controllers for HVDC lines. While the bulk power transmission network primarily uses alternating current (AC), HVDC lines are appealing for transmission of large amounts of power over long distances. Because they can alter operating points significantly, HVDC lines can have large impact on the stability and transient characteristics of power networks. Also, the integration of solid-state power electronics and synchrophasors is enabling sophisticated fast control of HVDC lines (known in the literature as HVDC *modulation*). However, experience shows that HVDC modulation needs to be undertaken with care, since these controls can introduce oscillations or leave the network susceptible to disruptions (see [9,10]). The analysis of control channels pursued here directly informs the design and analysis of HVDC modulation.

The research described here contributes to a recent research thrust on characterizing the zeros of canonical linear network models from a graph-theory perspective [11-15]. The initial studies in this direction were focused on models with scalar subsystem dynamics, and were subsequently extended to include models with homogeneous vector subsystems. Recently, we extended these studies to obtain algebraic and preliminary graph-theoretic results for the classical swing-dynamics model [6]. Here, we study the impact of in-built control schemes (specifically, HVDC controls) on input-output channel characteristics. Our research also builds on a wide literature which approach power-system small-signal and transient analysis from a graph-theory perspective (see e.g. [16-19]).

The rest of the article is organized as follows. In Section 2, the input-output swing-dynamics model is reviewed and enhanced to represent HVDC modulation. In Section 3, several graph-theoretic results on the zeros are given. An example is then presented to illustrate the results, and give an indication of parameter thresholds that distinguish minimum-phase and non-minimum-phase behaviors (Section 4).

2.2 Modeling

Input-output properties of the classical linearized swing dynamics model for the power transmission network are considered. The classical linearized swing dynamics model uses two state variables (the electrical angle and frequency relative to a reference) at the buses with inertial generators. A single input-output channel is imposed on the model, where the input is abstractly modeled as a power injection/extraction at a single bus, and the output is a frequency or angle measurement at a single (possibly different) bus. Formally, the following model is considered:

$$\begin{bmatrix}\dot{\delta}\\ \dot{\omega}\end{bmatrix} = \begin{bmatrix}0 & I\\ -H^{-1}L(\Gamma) & -H^{-1}D\end{bmatrix}\begin{bmatrix}\delta\\ \omega\end{bmatrix} + \begin{bmatrix}0\\ e_i\end{bmatrix}u \qquad (1)$$
$$y = \begin{bmatrix}0 & e_j^T\end{bmatrix}\begin{bmatrix}\delta\\ \omega\end{bmatrix}$$

where $\delta(t) = [\delta_1 \quad \cdots \quad \delta_n]^T$ represents the differential electrical angles at the n buses at time t (relative to a nominal trajectory), $\omega(t) = [\omega_1 \quad \cdots \quad \omega_n]^T$ represents the differential electrical frequencies at the buses, the notation e_q represents a 0-1 indicator vector with qth entry equal to 1, the scalar input $u(t)$ is a power-injection signal at bus i, and the scalar output $y(t)$ is the frequency at bus j. The model is defined by the following parameters: the positive diagonal matrix H represents the inertias of the generators at the buses, the positive diagonal matrix D captures the dampings of the generators, and the matrix $L(\Gamma)$ is a symmetric positive-definite or positive semi-definite matrix that entirely specifies the interactions among the buses. Importantly, the zero pattern and nonzero entries in the matrix $L(\Gamma)$ are commensurate with the topology of the power transmission network (equivalently, electrical connectivity among the buses), as specified by the graph Γ. Specifically, Γ is defined to be an undirected weighted graph whose vertices represent the buses. The edge weights are the susceptances of the lines connecting the buses, provided that the linearization is around a unloaded operating condition; when the linearization is around a non-zero operating point, the edge weights are instead the susceptances scaled by the cosine of the nominal electrical-angle difference between the vertices ([20]); these “effective susceptances" capture the changed stiffnesses in the swing dynamics. Each off-diagonal entry of the matrix $L(\Gamma)$ equals the negative of the edge weight between the corresponding vertices if there is an edge, and equals zero otherwise. The diagonal entries of $L(\Gamma)$ are positive, and at least as large as the absolute sum of the off-diagonal entries on the corresponding row or column. We assume throughout the article that Γ is connected.

For convenience, we use the notation A for the state matrix of the system, i.e. $A = \begin{bmatrix}0 & I\\ -H^{-1}L(\Gamma) & -H^{-1}D\end{bmatrix}$. We also find it convenient to define the state vector of the swing-dynamics model as $x = \begin{bmatrix}\delta\\ \omega\end{bmatrix}$. It can easily be checked that the matrix A is stable, in these sense that all eigenvalues are in the closed left half plane with no defective eigenvalues on the $j\omega$-axis. In fact, it can be checked that all eigenvalues of A are in the open-left half plane (OLHP), except that there is one eigenvalue at the origin in the special case that $L(\Gamma)$ is a true Laplacian matrix (all row sums are zero). The graph Γ is referred to as the **network graph**. Also, the nodes in the network where the input is applied and the output is measured (i and j, respectively) are referred to as the input and output nodes, and the corresponding vertices in the graph are referred to the the input and output vertices. The simplified model for the swing dynamics considered here is widely used in the power-engineering community, and constitutes a linearization of nonlinear Kuramoto oscillator-type model for the swing dynamics ([16-21]).

The formulation assumes that all buses have inertial generation associated with them, or in other words that the loads-only buses have been reduced via solution of the algebraic equations in the swing dynamics (which requires a Kron reduction). The graph Γ represents the interconnectivity of this reduced model, not the original topology including the load buses. We focus on this case with the aim of understanding input-output dynamics among the major swinging components of the wide-area network. Developing analyses of zeros in terms of the original rather than reduced network model is left to future work.

Here, the classical swing-dynamics model is extended to capture the fast dynamics of high-voltage direct-current (HVDC) lines in the network. The effects of HVDC line controllers on small-signal behaviors are more intricate, and require modifying the classical swing-dynamics modeling framework. Since controllers across HVDC lines have been shown to influence small-signal properties, a major focus of this work will be to model and evaluate possible HVDC line controllers. Broadly, the fast controlled HVDC line included network is different from classical swing-dynamics model by having 1) new state and/or 2) new dependencies between states (new nonzero entries in the state matrix). Small signal models for fast controlled HVDC have been described in ([26-28]). Here, four control schemes of increasing sophistication are modeled. We focus particularly on the case that the transfer function between the two ends of the HVDC line is of interest, i.e. the HVDC line is integrated between the input and output. This case is of particular interest because it shows whether or not inclusion of a HVDC line can improve small-signal characteristics across a channel of interest (typically one that is highly congested), and allow analysis of disruptions associated with the HVDC line. Here are the models:

1) A HVDC line with fixed power (no feedback regulation of power) does not alter the small-signal model, beyond changing graph edge weights (stiffnesses) due to the altered power flow.

2) a HVDC line with a general linear controller is considered. In this case, the power input is regulated using a linear feedback of the electrical phase angle difference across the DC line (in Laplace form $P_{q,r}(s) = kH(s)(\delta_q(s) - \delta_r(s))$, where $P_{q,r}$ is the differential power injection to bus r and extraction from bus q). Representing linear controllers in the swing-dynamics state-space model requires some new state variable, and new connections among state variables. The following is the linear swing-dynamics model with linear controller included. The full swing model can be expressed by enhancing the original model to include an additional dynamic feedback as $\begin{bmatrix}\delta \\ \omega\end{bmatrix} = \begin{bmatrix}0 & I \\ -H^{-1}L(\Gamma) & -H^{-1}D\end{bmatrix}\begin{bmatrix}\delta \\ \omega\end{bmatrix} + \begin{bmatrix}0 \\ -H^{-1}e_{q,r}\end{bmatrix}P_{q,r} + \begin{bmatrix}0 \\ e_i\end{bmatrix}u$ and the feedback in Laplace domain $P_{q,r}(s) = kH(s)(\delta_q(s) - \delta_r(s))$ where the notation $e_{q,r}$ represents a 0-1 indicator vector (with length n) with jth entry equal to 1, ith entry equal to -1, and the others equal to 0. In addition, the notation e_q represents a 0-1 indicator vector (with length n) with qth entry equal to 1 and the others equal to 0.

For example, a proportional-derivative controller may be used for HVDC modulation. In this case, the power input is regulated using a proportional-derivative (PD) feedback of the electrical phase angle difference across the DC line (in Laplace domain, $P_{qr}(s) = (k_p + k_d s)(\delta_r(s) - \delta_q(s))$, where P_{qr} is the differential power injection to bus q and extraction from bus r). A HVDC line with PD controller can be captured in the swing-dynamics model, by introducing new non-zero entries in the L matrix, and changing the D matrix. Specifically, if a PD-controlled HVDC line is

included between buses q and r, the linear swing dynamic model is modified by: 1) adding k_p to the entries $L_{q,q}$ and $L_{r,r}$ of L; 2) adding $-k_p$ to the entries $L_{q,r}$ and $L_{r,q}$ of L; 3) adding k_d to the entries $D_{q,q}$ and $D_{r,r}$ of D; 4) adding $-k_d$ to entries $D_{q,r}$ and $D_{r,q}$ of D. We call the updated L and D matrices as L_{DC} and D_{DC}, respectively. Hence, the linear model for this system is: $\begin{bmatrix}\delta \\ \omega\end{bmatrix} = \begin{bmatrix}0 & I \\ -H^{-1}L_{DC}(\Gamma) & -H^{-1}D_{DC}\end{bmatrix}\begin{bmatrix}\delta \\ \omega\end{bmatrix} + \begin{bmatrix}0 \\ e_i\end{bmatrix}u$ and $y = \begin{bmatrix}0 & e_j^T\end{bmatrix}\begin{bmatrix}\delta \\ \omega\end{bmatrix}$.

In practice, measurement delay may arise in HVDC line compensators, since they use remote measurements to govern the line power flow. In order to study the impact of the delay on the presence or absence of non-minimum-phase dynamics, the existing dynamic model is updated to represent the delay. For this initial effort, non-minimum phase transfer function approximations like (1,0)-Pade (1,1)-Pade approximations for the delay are used in the transfer-function analysis.

2.3 Results

Structural and graph-theoretic characterizations of the input-output swing-dynamics models enhanced with HVDC line controllers are obtained. The single-input single-output models considered here are fully characterized by their transfer functions. The transfer-function poles are internal properties of the state dynamics. These modal dynamics have been very extensively characterized in the power literature, including from a graph-theoretic perspective, and provide basic insight into the power network's small-signal dynamics. However, control design and disturbance analysis for dynamical systems crucially depend on the (finite) zeros of the transfer function, which are functions of the input-output channel in addition to the state dynamics. The importance of the zeros to control design and analysis stems from the fact that they are invariant to feedback, and hence their locations place fundamental limits on control performance. Particularly, control performance is distinguished by the presence and absence of right half plane (nonminimum phase) zeros. Thus, as wide-area control of the power transmission networks becomes increasingly feasible, and the networks are subject to increasing variability and disruption, characterizing the zeros of the swing-dynamics model is increasingly important. Numerical computation of the zeros for the classical model has been addressed by N. Martins and co-workers (see [8]) but few structural results are available, and the influences of dynamical components (e.g., HVDC line controllers, VSCs, etc) on the zeros are not well understood.

The main purpose of this section is to develop structural and graph-theoretic insights into the zeros of the swing-dynamics models enhanced models with HVAC controllers. The goal is to see how a modulated HVDC line will affect the zeros of the input-output model. A particular focus is on developing graph-theoretic sufficient conditions for the dynamics to be minimum phase (all finite zeros in the open left-half-plane) or non-minimum phase. The graph-theoretic analyses of zeros developed here are based on an algebraic transformation of linear systems known as the *special coordinate basis*. The special coordinate basis involves input, state, and output transformations of a linear system, which exposes its finite- and infinite- zero structures (see [22]). Specifically, the special coordinate basis separates a linear dynamics into integrator chains from inputs to outputs (which specify the infinite-zero structure), and a *zero dynamics* connected in feedback which captures the finite zero structure. Importantly, the transformation thus enables computation of the zeros as the eigenvalues of a *zeros state matrix*. This zeros state matrix turns out to equal a sparse

perturbation of a submatrix of the system's state matrix, where the nonzero entry locations in the perturbation are tied to the network's graph. This eigenvalue formulation for the zeros has been used to obtain several preliminary graph-theoretic results for the nominal swing-dynamics model in ([24]). The process requires extending the application of the special-coordinate-basis to encompass the models with HVDC controls.

For improved readability, proofs are placed after the presentation of results, in Section 2.6.

2.3.1 Analysis of Networks with Controlled HVDC Lines

Graph-theoretic results on the zeros of the swing-dynamics model are developed, for the case where controlled HVDC lines are present in the transmission network. Modern power transmission networks commonly include HVDC lines for stability and cost purposes. It is important to understand whether the integration of HVDC lines, and particularly the controls used on these lines, influence input-output behaviors in a power transmission network. In general, addition of an HVDC line may alter input-output channel properties throughout the network. As a first step, we study how the control on the HVDC line impacts the transfer function across the line (i.e., the transfer function when the input is the power injection on one end of the line, and the output is the frequency at the other end). This case is of particular interest because it gives insight into whether or not addition of an HVDC line between two buses improves the transfer characteristics for this channel, and also indicates the susceptibility of the HVDC control to disruption. In the following three theorems, we discuss the effect of HVDC line on zeros for different controllers applied across the line, focusing on specifying conditions that guarantee minimum-phase dynamics.

Theorem 1 *Consider the input-output swing dynamics model, in the case that there is a proportional-controlled HVDC line between the input and the output buses. If a sufficiently large proportional gain k is used on the HVDC line, the zeros of the system are in the OLHP except one zero at $s = 0$.*

Theorem 2 *Consider the input-output swing-dynamics model, with PD-controlled HVDC line between the input and the output vertices. If either the derivative gain k_d or the proportional gain k_p is large enough, the zeros of the model are in the OLHP except one zero at $s = 0$.*

Theorem 3 *Consider the input-output swing dynamics model, with a lead-compensated HVDC line between the input and output (specifically, a compensator of the form $P_{i,j} = k\frac{1+T_1 s}{1+T_2 s}(\delta_i - \delta_j)$). If the product kT_1 is sufficiently large (i.e. either k or T_1 is sufficiently large) and T_2 is sufficiently small, the zeros of the system are in the OLHP except one zero at $s = 0$.*

The impact of an HVDC line with strong control on other channels in the networks, where the input and output are not the ends of the HVDC, is also of significant interest. Since the HVDC line in this case can make alternative long paths from the input to the output strong, there is a possibility that the HVDC modulation may cause other channels to become non-minimum phase. The following theorems investigate the effect of an HVDC line on other channels in the networks, where the input and output might not be the ends of the HVDC. The following two theorems

discuss the cases where proportional-controlled HVDC line does not change the minimum phase behavior of the input-output swing dynamics channel.

Theorem 4 *Consider the input-output swing-dynamics model (1) for an arbitrary graph Γ. Assume that there is a proportional-controlled HVDC line between the two vertices r and q (i.e. $P_{q,r} = k(\delta_q - \delta_r)$). Suppose that in graph Γ, there is a single path between the input and output vertices. The input-output swing-dynamics model (1) with described HVDC modulation has all zeros in the OLHP except one zero at $s = 0$ if in graph Γ_{DC} there is a single path between the input and output vertices, i.e. adding an edge between vertices r and q in Γ does not add a second path between the input and output vertices.*

Next theorems require some further graph-theoretic notation for the network input-output model (1). In particular, let us a set of three vertices $V_d = \{i, j, n\}$ in the network graph. The vertex r is said to be a *disjointing vertex* of the set V_d if following paths pass through or reach the vertex r: 1) all paths from vertex i to vertex j, 2) all paths from vertex i to vertex n, 3) all paths from vertex j to vertex n. We note that the disjointing vertex may be one of the vertices in the set V_d. The concept of a disjointing vertex is illustrated in Fig. 1. In this example, vertex 1 is a disjointing vertex for the set $V_d = \{1,3,15\}$, vertex 2 is a disjointing vertex for both sets $V_{d_1} = \{1,2,15\}$ and $V_{d_2} = \{1,5,15\}$.

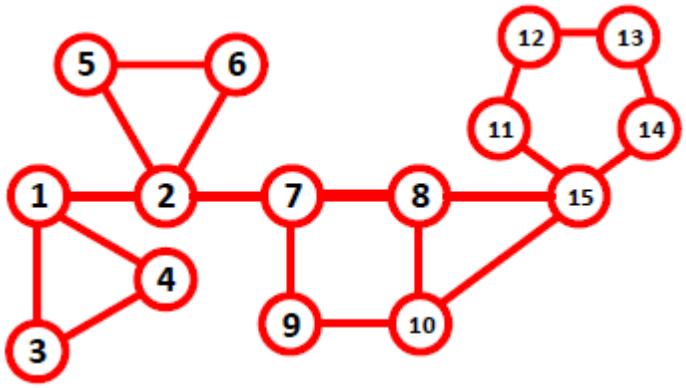

Figure 1: Graph Γ with several disjointing vertices, for example, vertex 1 is a disjointing vertex for the set $V_d = \{1,3,15\}$.

Theorem 5 *Consider the input-output swing-dynamics model (1) for an arbitrary graph Γ. Assume that there is a proportional-controlled HVDC line between the two vertices r and q (i.e. $P_{q,r} = k(\delta_q - \delta_r)$). Suppose that in associated graph Γ, there is a disjointing vertex for both sets $V_{d_1} = \{i, j, q\}$ and $V_{d_2} = \{i, j, r\}$. The input-output swing-dynamics model (1) with described HVDC modulation has zeros in ORHP similar to the input-output swing-dynamics model (1) without HVDC modulation.*

Now we discuss the case where HVDC lines with low-gain proportional controllers maintain the phase property. We note that an HVDC line with low-gain proportional controller necessarily only move system eigenvalues, and hence poles of any defined channel, by a small amount. In contrast,

they can introduce/remove zeros or cause zeros to jump in general. The graph-theoretic condition in the following Theorem is sufficient to guarantee that this does not happen, and hence that the phase property is maintained.

Theorem 6 *Consider the input-output swing-dynamics model (1) for an arbitrary graph Γ. Assume that there is a proportional-controlled HVDC line between the two vertices r and q (i.e. $P_{q,r} = k(\delta_q - \delta_r)$). Suppose that the distance from the input to output vertex in both associated graphs Γ and Γ_{DC} is the same, i.e. adding an edge between vertices r and q in Γ does not change the distance between input and output vertices. For all sufficiently small gains k, the input-output swing-dynamics model (1) with described HVDC modulation has zeros in the ORHP if the input-output swing-dynamics model (1) without HVDC modulation has zeros in the ORHP.*

The next two Theorems discuss the cases where a modulated HVDC line with low or high gain controller will cause ORHP zeros. First, a general condition is given such an HVDC line with low-gain dynamic controller change the phase property of the system to nonminimum phase by introducing ORHP zeros. The result shows that the ORHP zeros will be introduced when the location of the modulated HVDC line and the relative degree of the controller satisfy some conditions:

Theorem 7 *Consider the input-output swing-dynamics model (1), also assume a controlled HVDC line between the vertex q and r, i.e. $P_{q,r} = kH(s)(\delta_q - \delta_r)$ where the transfer function $H(s)$ has the relative degree equal to n_c. Suppose in graph Γ, we have $d_{iq} < d_{ir}$ and $d_{rj} < d_{qj}$. The input-output swing-dynamics model (1) with HVDC modulation has zeros in the ORHP:*

- for sufficiently small positive controller gain k, if $(d_{iq} + d_{rj} < d_{ij})$, $(2d_{iq} + 2d_{rj} + n_c + 5 \leq 2d_{ij})$, and $(n_c \geq -4)$.
- for sufficiently small negative controller gain k, if $(d_{iq} + d_{rj} < d_{ij})$, $(2d_{iq} + 2d_{rj} + n_c + 3 \leq 2d_{ij})$, and $(n_c \geq -2)$.

Next, a simple result is given which shows that a modulated HVDC line with high-gain nonminimum-phase controller or a low-gain unstable controller necessarily makes all remote channels nonminimum phase by introducing ORHP zeros. While it is not typical to use nonminimum-phase or unstable controllers, there is some motivation for studying these cases. First, the presence of delays and other unmodeled dynamics in the controller implementation may introduce nonminimum-phase characteristics in the feedback block, whose impacts across the network are of interest. Also, in some special cases, unstable or nonminimum-phase controllers are indeed needed. The analyses for these special cases are also a starting point for characterization of more commonly used controllers, developed subsequently.

Theorem 8 *Consider the input-output swing-dynamics model (1), also assume a controlled HVDC line between the vertex q and r, i.e. $P_{q,r} = kH(s)(\delta_q - \delta_r)$. The input-output swing-dynamics model (1) with HVDC modulation has zeros in the ORHP:*

- for sufficiently large gain k, if the transfer function $H(s)$ is non-minimum-phase.
- for sufficiently small gain k, if the transfer function $H(s)$ is unstable.

The main concept underlying the result is that the zeros of remote channels approach the HVDC line controller's zeros when a high-gain feedback is used. Also, the zeros of remote channels approach the HVDC line controller's poles when a low-gain feedback is used. For the cases discussed in the previous theorem, we note that a high-gain control also can make the system unstable (i.e. poles are driven into the right half plane), however, nonminimum-phase behaviors may appear before instability occurs in these circumstances.

In practice, HVDC line controllers may be subject to measurement delay, since they use remote measurements to govern the line power flow. In the next theorems, we study the impact of the delay on the presence or absence of non-minimum-phase dynamics, using (1,0) and (1,1) Pade approximations for the delay in the transfer-function analysis. The main outcome of this analysis is show that proportional and lag compensation schemes with sufficient gain yield non-minimum-phase transfer functions, if measurement delays are present.

Theorem 9 *Consider the input-output swing-dynamics model (1), also assume a controlled HVDC line between the vertex q and r, i.e. $P_{q,r} = kH(s)(\delta_q - \delta_r)$. For sufficiently large control gain k, input-output swing-dynamics model (1) with HVDC modulation is non-minimum-phase if controller is subject to measurement delay and it can be approximated by a non-minimum-phase transfer function $H(s)$.*

Theorem 10 *Consider the input-output swing-dynamics model with proportional-controlled HVDC line between input and output, where the controller is subject to a measurement delay T_1. The compensator with delay can be approximated as $P_{i,j} = k(1 - T_1 s)(\delta_i - \delta_j)$, where a (1,0) Pade approximation has been used for the delay. If the proportional gain k of the HVDC line is sufficiently large, one of the zeros of the system will be in the ORHP, i.e. the system will be non-minimum-phase.*

Theorem 11 *Consider the input-output swing-dynamics model with proportional-controlled HVDC line between input and output, where the controller is subject to a measurement delay T_d. The compensator with delay can be approximated as $P_{i,j} = k\frac{(1-0.5T_d s)}{(1+0.5T_d s)}(\delta_i - \delta_j)$, where a (1,1)-Pade approximation has been used for the delay. If the proportional gain k of the HVDC line is sufficiently large and delay T_d is sufficiently small, one of the zeros of the system will be in the ORHP, i.e. the system will be non-minimum-phase.*

Theorem 12 *Consider the input-output swing dynamics model with lag-controlled HVDC line between input and output, where the controller is subject to a measurement delay T_d. The compensator with delay can be approximated as $P_{i,j} = k\frac{1-T_d s}{1+T_2 s}(\delta_i - \delta_j)$, where the (1,0) Pade approximation has been used for the delay. If kT_d is sufficiently large (i.e. either k or T_d are sufficiently large), and T_2 is sufficiently small, one of zeros of the system will be in the ORHP, so the system is non-minimum-phase.*

While the analyses here are based on the Pade approximation, we hypothesize that the results carry through to an exact model of the delay. We expect to pursue this analysis in further work.

2.4 Example

A small-scale example with six buses is used to illustrate the results on transmission networks with HVDC modulation (Figure 2). The channel of interest comprises an input at bus 1 and output at bus 3. The generator at each bus has inertia $h = 1$ and damping $d = 0.2$, and the edge weights (effective line susceptances) are shown in the figure. Let us assume that there is a HVDC line between bus 1 and 3. Out goal is to study the effect of the HVDC controller's parameters on the zero location. In addition, we study how the threshold on the control parameters for minimum-phase behavior depends on other characteristics of the network (e.g., damping, susceptances). To examine these dependencies, in each subplot in Fig. 3 and Fig. 4, we plot the largest real part among the zeros as a function of a control parameter, for different values of the network's parameters. In Fig. 3, the plots in different colors represent different effective susceptances β. In Fig. 4, the plots in different colors represent different damping levels (d), which are uniform for all generators in the network. For convenience, as discussed before, the zeros of system are computed for the case that the output is δ_3 instead of ω_3 (since the frequency output will simply introduce one further zero at the origin).

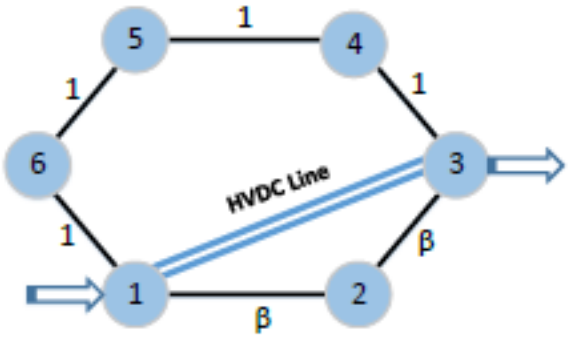

Figure 2: A 6-bus example network

Second, a lead-compensated HVDC line is considered. First, two controller parameters are fixed at $k = 0.2$ and $T_2 = 0.2$, and the effect of T_1 on the zero location is investigated, see Figure 3(c) and Figure 4(c). As expected, the system is minimum phase for large T_1. Alternately, two parameters are fixed at $k = 0.2$ and $T_1 = 20$, and the effect of the remaining parameter T_2 is investigated. As expected, the system is minimum phase for small T_2, see Figure 3(d) and Figure 4(d).

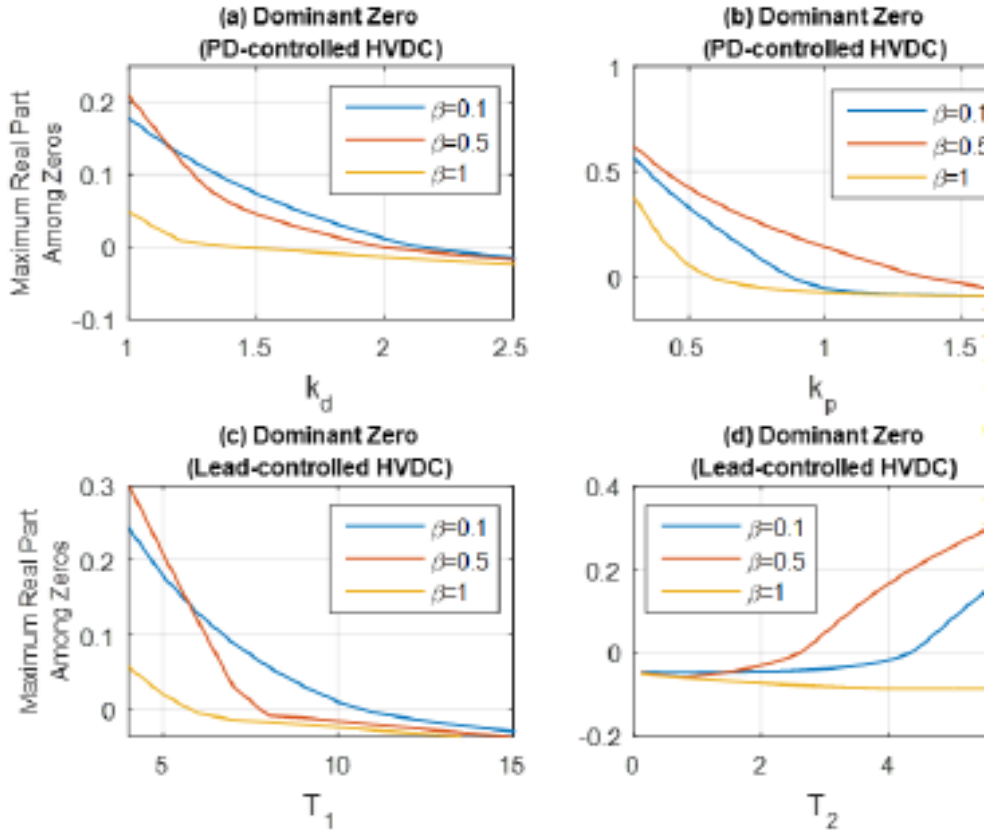

Figure 3: The dependences of the dominant zero's location on the controller parameters are shown, for three different values of the effective line susceptance.

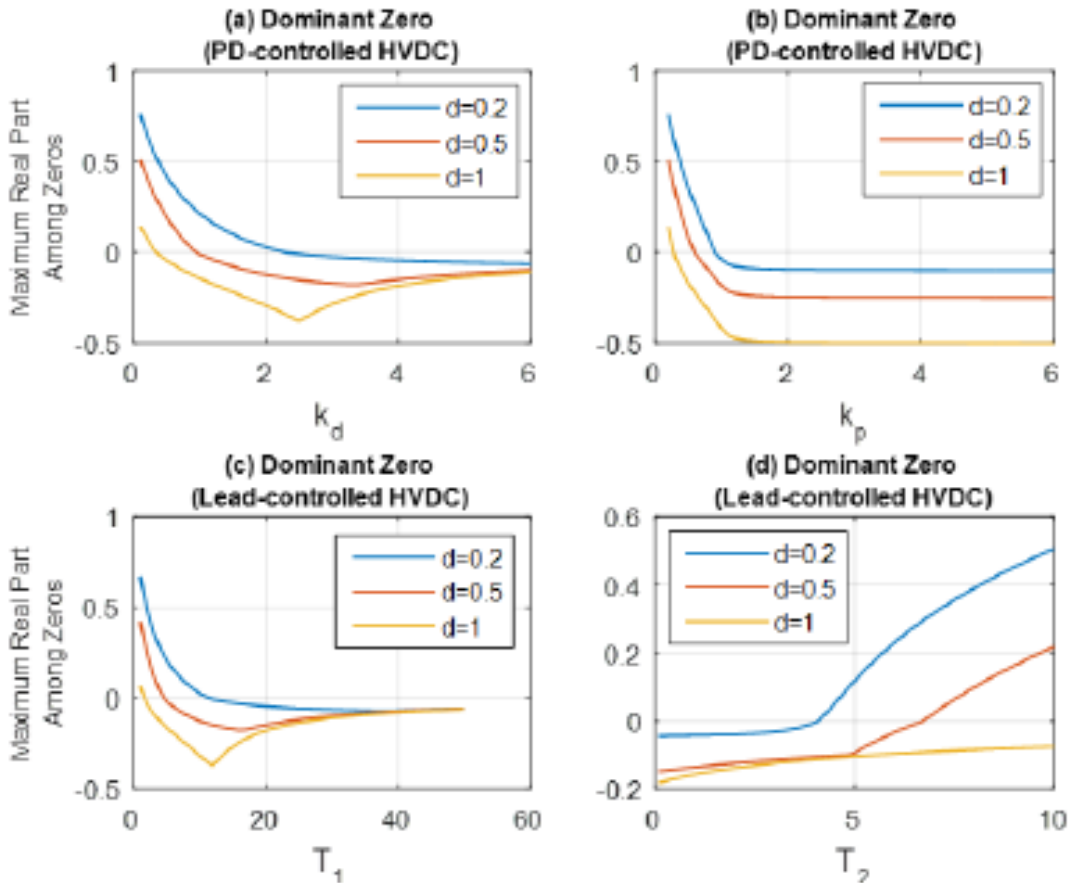

Figure 4: The dependences of the dominant zero's location on the controller's parameters are shown, for three different damping levels.

2.5 Discussion

Input-output properties (specifically, zero locations) of the bulk power system's swing dynamics have been examined from a graph-theory standpoint. The impacts of HVDC modulation on the zeros has also been studied. The analyses show that the zero locations, and particular the presence or absence of non-minimum-phase zeros, is strongly connected to the network's topology and structural parameters. Strong HVDC controllers (specifically, proportional and proportional-derivative controllers) make collocated input-output channels minimum-phase, which indicates the benefit of such modulation for control of fast dynamics. However, measurement delays on these strong HVDC controllers are shown to yield non-minimum-phase dynamics, which confirms

that HVDC modulation must be undertaken with care. An important direction of future work is to understand how HVDC integration influences other control channels in the transmission network.

2.6 Proofs of Formal Results

Proof of Theorem 1: The swing dynamics upon addition of a proportional-controlled HVDC line is governed by:

$$\begin{bmatrix}\delta\\ \omega\end{bmatrix} = \begin{bmatrix}0 & I\\ -H^{-1}L_{DC}(\Gamma) & -H^{-1}D\end{bmatrix}\begin{bmatrix}\delta\\ \omega\end{bmatrix} + \begin{bmatrix}0\\ e_i\end{bmatrix}u \qquad (2)$$
$$y = \begin{bmatrix}0 & e_j^T\end{bmatrix}\begin{bmatrix}\delta\\ \omega\end{bmatrix},$$

where L_{DC} is defined in Section 2. We notice that the model with the proportional-controlled HVDC line has the same form as the model without the HVDC line, but with an additional effective susceptance k included in the model between i and j (the input and output, which are also the ends of the HVDC line). In particular, we notice that L_{DC} maintains the grounded Laplacian structure of L, but with an additional HVDC line included. Thus, if the gain k is large enough, it follows directly from Theorem 5 in [4] that the dynamics is minimum phase. ■

Proof of Theorem 4: The described HVDC line with proportional control can be captured in the input-output swing-dynamics model (1) by including additional non-zero entries in L matrix, identically to a newly added AC line. Precisely, when a proportional-controlled HVDC line with gain k is included between buses q and r, the nominal linear swing dynamic models is modified by adding k to $L_{q,q}$ and $L_{r,r}$ and adding $-k$ to $L_{q,r}$ and $L_{r,q}$. In this case, the linearized model of the HVDC line is identical to that of an AC line. Using the notation L_{DC} for the modification of the L matrix, the swing-dynamics model becomes: $\begin{bmatrix}\delta\\ \omega\end{bmatrix} = \begin{bmatrix}0 & I\\ -H^{-1}L_{DC}(\Gamma) & -H^{-1}D\end{bmatrix}\begin{bmatrix}\delta\\ \omega\end{bmatrix} + \begin{bmatrix}0\\ e_i\end{bmatrix}u$ and $y = \begin{bmatrix}0 & e_j^T\end{bmatrix}\begin{bmatrix}\delta\\ \omega\end{bmatrix}$.

The associated graph Γ_{DC} for this system can be developed by adding an edge between vertices q and r in graph Γ. Based on the result from earlier theorems, the input-output swing-dynamics when there is a single path between input and output vertices in graph Γ_{DC}, then the input-output swing-dynamics model has all zeros in the OLHP, except one zero at $s = 0$. ■

Proof of Theorem 5: The described HVDC line with proportional control can be captured in the input-output swing-dynamics model (1) by including additional non-zero entries in L matrix, identically to a newly added AC line. Precisely, when a proportional-controlled HVDC line with gain k is included between buses q and r, the nominal linear swing dynamic models is modified by adding k to $L_{q,q}$ and $L_{r,r}$ and adding $-k$ to $L_{q,r}$ and $L_{r,q}$. In this case, the linearized model of the HVDC line is identical to that of an AC line. Using the notation L_{DC} for the modification of the L matrix, the swing-dynamics model becomes: $\begin{bmatrix}\delta\\ \omega\end{bmatrix} = \begin{bmatrix}0 & I\\ -H^{-1}L_{DC}(\Gamma) & -H^{-1}D\end{bmatrix}\begin{bmatrix}\delta\\ \omega\end{bmatrix} + \begin{bmatrix}0\\ e_i\end{bmatrix}u$ and $y = \begin{bmatrix}0 & e_j^T\end{bmatrix}\begin{bmatrix}\delta\\ \omega\end{bmatrix}$. In addition, the associated graph Γ_{DC} for this system can be developed by adding an edge between vertices q and r in graph Γ. In following we discuss matrices A_{n_a}, A_q, and A_{aa} for state matrix A with L_{DC}.

Considering the assumption about existing a disjointing vertex for both sets $V_{d_1} = \{i, j, q\}$ and $V_{d_2} = \{i, j, r\}$, we can say that in graph Γ_{DC}, there is a vertex on special input-output path called t that is a disjointing vertex for both sets V_{d_1} and V_{d_2}.

To prove the result, we show that the matrix A_{aa} is a strictly block upper-triangular matrix that has two block submatrices. Only one of the block submatrix might have ORHP eigenvalues which the HVDC gain has no effect on this block submatrix. Hence, changing the HVDC gain k, does not move the ORHP zeros of the input-output model.

Let us call vertices included in special input-output path as special vertices, and call the other vertices as non-special vertices. In addition, let us call edges in special input-output path as special edges and the others as non-special edges. We partition the non-special vertices into two disjoint subsets. First subset V_1 contains the non-special vertices that vertex t is the special vertex for the set of each one of those vertices, vertex i, and vertex j. In other word, in graph Γ, each path from the vertices in first subset to vertex i or j will pass through vertex t. The second subset V_2 contains the remaining non-special vertices that are not in the first subset. Without loss of generality, we assume that the non-special vertices are ordered according to the subsets (i.e., the vertices in $v_1^{(1)}$ are first, then those in $v_1^{(2)}$. Assuming this ordering, we notice that A_{n_a} is block diagonal matrix, with the diagonal blocks $A_{n_a} = \begin{matrix} A_{n_a}(V_1) & 0 \\ 0 & A_{n_a}(V_2) \end{matrix}$ corresponding to each subset v_1 and V_2. Let us now consider the perturbation A_q. Based on the results from Theorems 3 and 4 in [4], one can easily show that the perturbation matrix A_q has non-zero entries only the the rows corresponding to vertices V_2, i.e. $A_q = \begin{matrix} A_q(V_1) & A_q(V_{1,2}) \\ 0 & 0 \end{matrix}$. Hence the matrix A_{aa} can be written as $A_{aa} = \begin{matrix} A_{n_a}(V_1) + A_q(V_1) & A_q(V_{1,2}) \\ 0 & A_{n_a}(V_2) \end{matrix}$. One can easily show that the HVDC gain k only affect the submatrix $A_{n_a}(V_2)$. In addition, we know that matrix A_{n_a} has all eigenvalues in OLHP except one in $s = 0$, so submatrix $A_{n_a}(V_2)$ also has all eigenvalues in OLHP and at most one eigenvalue at $s = 0$. On the other hand, the matrix $A_{n_a}(V_1) + A_q(V_1)$ might have eigenvalues in ORHP. Hence, by changing the HVDC gain k, the OLHP zeros of the input-output swing-dynamics model with HVDC modulation does not move to the OLHP. ■

Proof of Theorem 6: Similar to the proof for theorem 4, the proportional controller $P = ke_q(x_j - x_q)$ can be captured in the input-output model without controller as: $\begin{bmatrix} \delta \\ \omega \end{bmatrix} = \begin{bmatrix} 0 & I \\ -H^{-1}L_{DC}(\Gamma) & -H^{-1}D \end{bmatrix} \begin{bmatrix} \delta \\ \omega \end{bmatrix} + \begin{bmatrix} 0 \\ e_i \end{bmatrix} u$ and $y = \begin{bmatrix} 0 & e_j^T \end{bmatrix} \begin{bmatrix} \delta \\ \omega \end{bmatrix}$

From Theorem 1, the zeros of the input-output swing-dynamics model (1) are the eigenvalues of the matrix $A_{aa} = A_{n_a} + A_q$, where A_{n_a} is the principal submatrix of state matrix A corresponding to the nodes that are not on the special input-output path, and A_q is a perturbation matrix. Likewise, considering $\tilde{A}$ as the modified state matrix with L_{DC}, the zeros of the system with HVDC modulation are the eigenvalues of the matrix $\tilde{A}_{aa} = \tilde{A}_{n_a} + \tilde{A}_q$, where $\tilde{A}_{n_a}$ is the principal submatrix of $\tilde{A}$ corresponding to the nodes that are not on the special input-output path, and $\tilde{A}_q$ is

a perturbation matrix. From the assumption that the distance between the input and output is unchanged in the modified graph Γ_{DC} as compared to the original graph Γ, it follows that both models have the same special input-output path. Hence, A_{n_a} and $\tilde{A}_{n_a}$ are corresponding principal submatrices of the matrix A and $\tilde{A}$. Thus, as the gain k is made small, the entries in A_{n_a} and $\tilde{A}_{n_a}$ become arbitrarily close to each other. Using the fact that the special input-output path is maintained, it can similarly be argued that corresponding expressions can be used to find the perturbations A_q and $\tilde{A}_q$, and in turn that these perturbations are close for small k (the details of the algebra are omitted to simplify the presentation). It thus follows that the controlled system has the same number of zeros as the uncontrolled one, and further the zeros become arbitrarily close as the gain k is decreased, from continuity of eigenvalues to matrix entries. Thus, the phase property is maintained for all sufficiently small gain k (i.e. for all $|k| < f$ for some threshold $f < \infty$). ■

Proof of Theorem 2: To prove this theorem, we develop the special coordinate basis for the network with a PD-controlled HVDC line between input and output vertices. For this purpose, first we discuss the swing-dynamics model for this case. In case of HVDC modulation with a proportional-derivative controller, the power input is regulated using a proportional-derivative (PD) feedback of the electrical phase angle difference across the DC line (in Laplace domain, $P_{in}(s) = (k_p + k_d s)(\delta_j(s) - \delta_i(s))$, where P_{in} is the differential power injection to bus i and extraction from bus j). A HVDC line with PD controller can be captured in the swing-dynamics model, by introducing new non-zero entries in the L matrix, and changing the D matrix. Specifically, if a PD-controlled HVDC line is included between buses i and j, the linear swing dynamic model is modified by: 1) adding k_p to the entries $L_{i,i}$ and $L_{j,j}$ of L; 2) adding $-k_p$ to the entries $L_{i,j}$ and $L_{j,i}$ of L; 3) adding k_d to the entries $D_{i,i}$ and $D_{j,j}$ of D; 4) adding $-k_d$ to entries $D_{i,j}$ and $D_{j,i}$ of D. We call the updated L and D matrices as L_{DC} and D_{DC}, respectively. Hence, the linear model for this system is:

$$\begin{bmatrix}\delta \\ \omega\end{bmatrix} = \begin{bmatrix}0 & I \\ -H^{-1}L_{DC}(\Gamma) & -H^{-1}D_{DC}\end{bmatrix}\begin{bmatrix}\delta \\ \omega\end{bmatrix} + \begin{bmatrix}0 \\ e_i\end{bmatrix}u \qquad (3)$$
$$y = \begin{bmatrix}0 & e_j^T\end{bmatrix}\begin{bmatrix}\delta \\ \omega\end{bmatrix}$$

Now let us develop the special coordinate basis for the network with a PD-controlled HVDC line between input and output vertices. In this network, the relative degree of system is equal to $n_d = 2$, and therefore $n_a = 2n - n_d = 2n - 2$. In using the special coordinate basis, we find it convenient to make the following assumptions: 1) For the network with n nodes, we assume output node is labeled $n-1$ and the input node which is also connected to the PD-controlled HVDC line is labeled n. 2) Let us assume the following particular ordering of the original state vector and the corresponding graph vertices.

$$x = [\delta_1 \quad \omega_1 \quad \cdots \quad \delta_{n-2} \quad \omega_{n-2} \quad \delta_{n-1} \quad \delta_n \quad \omega_{n-1} \quad \omega_n]^T \qquad (4)$$

We can easily find the matrix A_{n_a} and the perturbation matrix A_q. In matrix A_{n_a}, the two last rows (rows corresponding to δ_{n-1} and δ_n) are equal to zero for all entries. In the matrix A_q, all the rows except the last row are equal to zero. On the other hand, in the last row of A_q, all the entries are proportional to k_d^{-1}. In addition, only the entries of the last two columns in the last row of A_q are

related to k_p. To make it more clear, let us assume that node $n-1$ is only connected to node $n-2$ and try to express the dependence of matrix A_q on k_p and k_d as:

$$A_q = \begin{bmatrix} 0 & 0 & & 0 & 0 & 0 & 0 \\ \vdots & \vdots & \ddots & \vdots & \vdots & \vdots & \vdots \\ 0 & 0 & & 0 & 0 & 0 & 0 \\ 0 & 0 & & \frac{L_{4,5}}{k_d} & 0 & \frac{-L_{4,5}+k_p}{k_d} & \frac{-k_p}{k_d} \end{bmatrix} \quad (5)$$

where $L_{4,5}$ is the entry of matrix L and is negative value. By $A_{aa} = A_{n_a} + A_q$, if either the gain k_d or the gain k_p is large enough, the A_{aa} matrix will become close to a block upper-triangular matrix with two diagonal blocks. The size of the first block is $(2n-4) \times (2n-4)$,and the size of the second block is 2×2. In addition, the entries of first block are corresponding entries of A_{n_a} without any perturbation, so its eigenvalues are all in the OLHP. On the other hand, the second block is in the form of $\begin{bmatrix} 0 & 0 \\ \frac{-L_{4,5}+k_p}{k_d} & \frac{-k_p}{k_d} \end{bmatrix}$, so its eigenvalues are one at zero $s = 0$ and the other one $s = \frac{-k_p}{k_d}$ which is in OLHP. In summary, if either the gain k_d or the gain k_p is large enough, the zeros of the system will be in the OLHP except one zero at $s = 0$. ■

Proof of Theorem 3: To prove this theorem, we develop the special coordinate basis for the network with a HVDC line with a lead-lag compensator between input and output vertices. For this purpose, first we discuss the swing-dynamics model for this case. In this case, the power input is regulated using a lead-lag compensated feedback of the electrical phase angle difference across the DC line (in Laplace form $P_{in}(s) = k\frac{1+T_1 s}{1+T_2 s}(\delta_j(s) - \delta_i(s))$, where P_{in} is the differential power injection to bus i and extraction from bus j). Representing lead-lag controllers in the swing-dynamics state-space model requires a new state variable, and new connections among state variables. The following is the linear swing-dynamics model with lead compensator included. The full swing model can be expressed by enhancing the original model to include an additional dynamic feedback:

$$\begin{bmatrix} \delta \\ \omega \end{bmatrix} = \begin{bmatrix} 0 & I \\ -H^{-1}L(\Gamma) & -H^{-1}D \end{bmatrix} \begin{bmatrix} \delta \\ \omega \end{bmatrix} + \begin{bmatrix} 0 \\ -H^{-1}e_{j,i} \end{bmatrix} P + \begin{bmatrix} 0 \\ e_i \end{bmatrix} u \quad (6)$$

$$T_2 \dot{P} = -P + k\begin{bmatrix} e_{j,i}^T & T_1 e_{j,i}^T \end{bmatrix} \begin{bmatrix} \delta \\ \omega \end{bmatrix}, y = \begin{bmatrix} 0 & e_j^T \end{bmatrix} \begin{bmatrix} \delta \\ \omega \end{bmatrix}$$

where the notation $e_{j,i}$ represents a 0-1 indicator vector (with length n) with jth entry equal to 1, ith entry equal to -1, and the others equal to 0. In addition, the notation e_q represents a 0-1 indicator vector (with length n) with qth entry equal to 1 and the others equal to 0.

We simplify the described model as a new state space model with $2n+1$ states, including all δ_i, ω_i, and a new state P. Now, let us apply the transformation to the special coordinate basis. For described network, the relative degree of system is equal to $n_d = 3$, so $n_a = 2n-2$. Let us assume the following particular ordering of the original state vector and the corresponding graph vertices.

$$x = [\delta_1 \quad \omega_1 \quad \cdots \quad \delta_{n-2} \quad \omega_{n-2} \quad \delta_{n-1} \quad \delta_n \quad \omega_{n-1} \quad P \quad \omega_n]^T \quad (7)$$

By using the previous theorems, we can easily find the matrix A_{n_a} and perturbation matrix A_q. In the matrix A_{n_a}, the entries of two last rows (rows corresponding to δ_{n-1} and δ_n) are equal to zero.

In the matrix A_q, all the rows except the last one are equal to zero. In addition, the dependence of matrix A_q on T_1, T_2, and k can be shown as:

$$A_q = \begin{bmatrix} 0 & 0 & \ddots & 0 & 0 & 0 & 0 \\ \vdots & \vdots & & \vdots & \vdots & \vdots & \vdots \\ 0 & 0 & & 0 & 0 & 0 & 0 \\ a_{(2n-3)} + b_{(2n-3)} & a_{(2n-4)} & & a_3 + b_3 & a_2 & \frac{-1}{T_1} + a_1 + b_1 & \frac{-1}{T_1} \end{bmatrix}$$

where $a_r = \gamma_r * \frac{T_2}{kT_1}$ and $b_r = \beta_r * \frac{1}{kT_1}$ with γ_r and β_r independent of T_1, T_2, and k. By considering $A_{aa} = A_{n_a} + A_q$, for sufficiently large kT_1 (i.e. either k or T_1 is sufficiently large), and sufficiently small T_2 (precisely sufficiently small $\frac{T_2}{kT_1}$), the A_{aa} matrix will be close to a block upper-triangular matrix with two block diagonals. The size of the first block is $(2n-4) \times (2n-4)$ and the size of the second block is 2×2. In addition, the entries of first block are corresponding entries of A_{n_a} without any perturbation, so its eigenvalues are all in the OLHP. On the other hand, the second block is in the form of $\begin{bmatrix} 0 & 0 \\ \frac{-1}{T_1} & \frac{-1}{T_1} \end{bmatrix}$, so its eigenvalues are one at zero and the other one $\frac{-1}{T_1}$. In summary, for sufficiently large kT_1 (i.e. either k or T_1 is sufficiently large), and sufficiently small T_2 (precisely sufficiently small $\frac{T_2}{kT_1}$), the zeros of the system are in the OLHP except one zero at $s = 0$. ■

Proof of Lemma 7: The proof depends on an appropriate block-diagram representation of the input-output swing-dynamics model (1) with HVDC modulation (see Fig. 5). Further, we consider the same subsystems and notation used in the proof for Theorem 8. The transfer functions H_1, H_2, H_3, and H_4 have relative degrees $2d_{iq} + 2$, $2d_{rj} + 1$, $2d_{ij} + 1$, and $2d_{rq} + 2$ respectively, and all of them have positive gain. From the proof of Theorem 8, the zeros of $H(s)$ are the roots of equation $b_1 b_2 a_3 b_4 b_u + k a_u (a_1 a_2 b_3 b_4 - b_1 b_2 a_3 a_4) = 0$.

If $(d_{iq} + d_{rj} < d_{ij})$, it is easy to show that $\deg(a_1 a_2 b_3 b_4) > \deg(b_1 b_2 a_3 a_4)$ so $\deg(a_1 a_2 b_3 b_4 - b_1 b_2 a_3 a_4) = \deg(a_1 a_2 b_3 b_4)$. On the other hand, based on the fact that $(2d_{iq} + 2d_{rj} + \boldsymbol{n_c} + 5 \leq 2d_{ij})$, we have $\deg(b_1 b_2 a_3 b_4 b_u) + 3 \leq \deg(a_u (a_1 a_2 b_3 b_4 - b_1 b_2 a_3 a_4))$. Therefore, the root-locus has at least one diverging branch at the RHP. Consequently, for a sufficiently small positive HVDC gain k, the roots of equation $b_1 b_2 a_3 b_4 b_u + k a_u (a_1 a_2 b_3 b_4 - b_1 b_2 a_3 a_4) = 0$ are very close to the roots of $b_1 b_2 a_3 b_4 b_u = 0$ and at least one zero at right half plane. Following a similar analysis, one can prove that the condition $(\boldsymbol{n_c} \geq -4)$ is required to guarantee that $H(s)$ is stable for a sufficiently small positive HVDC gain k if transfer function $H_u(s)$ is stable.

For small negative gain, similar to previous part, based on the fact that $(2d_{iq} + 2d_{rj} + \boldsymbol{n_c} + 3 \leq 2d_{ij})$, we have $\deg(b_1 b_2 a_3 b_4 b_u) + 1 \leq \deg(a_u (a_1 a_2 b_3 b_4 - b_1 b_2 a_3 a_4))$. Therefore, the (negative) root-locus has at least one diverging branch at the RHP. Consequently, for a sufficiently small negative HVDC gain k, the roots of equation $b_1 b_2 a_3 b_4 b_u + k a_u (a_1 a_2 b_3 b_4 - b_1 b_2 a_3 a_4) = 0$ are very close to the roots of $b_1 b_2 a_3 b_4 b_u = 0$ and at least one zero at right half plane. Following a similar analysis, one can prove that the condition $(\boldsymbol{n_c} \geq -2)$ is required to guarantee that $H(s)$ is stable for a sufficiently small negative HVDC gain k if transfer function $H_u(s)$ is stable. ■

Proof of Theorem 8: The proof depends on an appropriate block-diagram representation of the transfer function from u to y in the network input-output swing-dynamics model (1) with HVDC modulation. For this theorem, a controller that measures $\delta_q - \delta_r$ and actuates both nodes q and r is considered. The network input-output swing-dynamics model (1) with HVDC modulation can be expressed in terms of the following two interconnected subsystem models:

Subsystem S_1, which has two inputs (i.e. u and P) and two output (i.e. y and z), is governed by: $\begin{bmatrix}\delta \\ \omega\end{bmatrix} = \begin{bmatrix}0 & I \\ -H^{-1}L(\Gamma) & -H^{-1}D\end{bmatrix}\begin{bmatrix}\delta \\ \omega\end{bmatrix} + \begin{bmatrix}0 \\ -H^{-1}(e_q - e_r)\end{bmatrix}P + \begin{bmatrix}0 \\ e_i\end{bmatrix}u$ and $y = \begin{bmatrix}0 & e_j^T\end{bmatrix}\begin{bmatrix}\delta \\ \omega\end{bmatrix}$ and $z = \delta_q - \delta_r$.

Subsystem S_2, which has one input (i.e. z) and one output (i.e. P) with transfer function $P(s) = kH(s)Z(s)$.

In this case, it is convenient to decompose the transfer function from u to y as shown in the block diagram in Fig. 5.

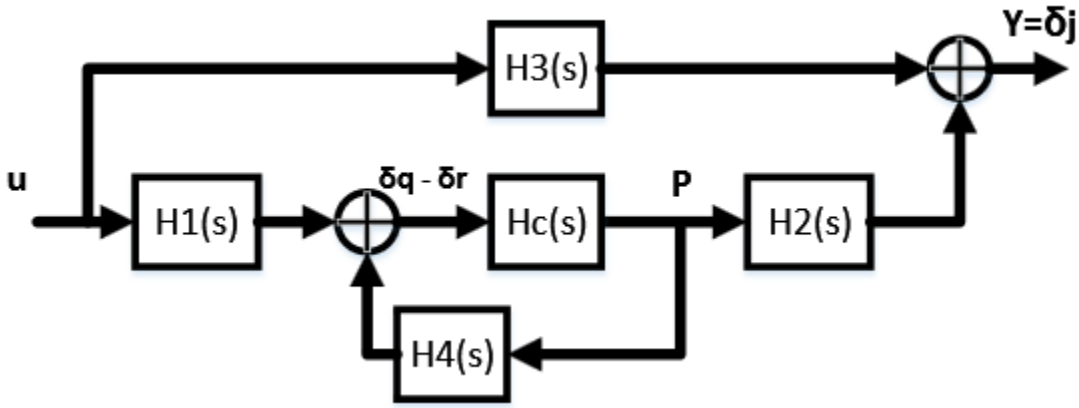

Figure 5: Block-diagram representation for the system presented in the proof of Theorem 8.

In the block diagram (Fig. 5), $H_3(s) = \frac{Y(s)}{U(s)}$ and $H_1(s) = \frac{Z(s)}{U(s)} = \frac{\delta_q(s) - \delta_r(s)}{U(s)}$ are the transfer functions defined for subsystem S_1, and $H_c(s) = kH_u(s)$ is the subsystem S_2 or controller transfer function (as assumed in the theorem statement). Further, the diagram explicitly denotes the output of the controller as P which drives the generator q and r. Also in subsystem S_1, $H_2(s)$ represents the transfer function from a putative input P at vertices q and r (e.g., the actuation given by the built controller) to the output y which is the state at vertex j (i.e., ω_j) while $H_4(s)$ is the transfer function from the putative input P at vertices q and r to the state of the vertex j (i.e. ω_j). Equivalence with the closed-loop network input-output model is immediate from linearity.

From the block diagram, the transfer function for the closed-loop system is:

$$\begin{aligned} H(s) &= \frac{Y(s)}{U(s)} \\ &= H_3(s) + \frac{H_1(s)H_c(s)H_2(s)}{1-H_c(s)H_4(s)} \\ &= \frac{H_3(s)+H_c(s)[H_1(s)H_2(s)-H_3(s)H_4(s)]}{1-H_c(s)H_4(s)} \\ &= \frac{H_3(s)+kH_u(s)[H_1(s)H_2(s)-H_3(s)H_4(s)]}{1-kH_u(s)H_4(s)} \end{aligned} \tag{8}$$

Consider $H_i(s) = \frac{a_i(s)}{b_i(s)}$ for $i \in \{1,2,3,4,u\}$, where $a_i(s)$ and $b_i(s)$ are the polynomials in nominator and denominator of $H_i(s)$ and we drop the Laplace-transform variable s to make the presentation clearer. In this notation, the closed-loop transfer function H can be written as:

$$\begin{aligned} H &= \frac{H_3+kH_u(H_1H_2-H_3H_4)}{1-kH_uH_4} \\ &= \frac{b_1b_2a_3b_4b_u+ka_u(a_1a_2b_3b_4-b_1b_2a_3a_4)}{b_1b_2b_3b_4b_u-ka_ub_1b_2b_3a_4} \end{aligned} \tag{9}$$

Hence, the poles of transfer function $H(s)$ are the roots of the following equation:

$$b_1b_2b_3(b_4b_u - ka_ua_4) = 0 \tag{10}$$

and the zeros of transfer function $H(s)$ are the roots of:

$$b_1b_2a_3b_4b_u + ka_u(a_1a_2b_3b_4 - b_1b_2a_3a_4) = 0 \tag{11}$$

From a root-locus analysis, for sufficiently large gain k, some of the poles and zeros of $H(s)$ are very close to the roots of $a_u(s) = 0$. Hence, for sufficiently large gain k, the input-output model is nonminimum phase as well as unstable if $H_u(s)$ is assumed to be nonminimum phase. Note that maybe by increasing gain k, first nonminimum-phase behavior appears and then instability occurs. In a similar way, via a root-locus analysis, it can be shown that $H(s)$ has poles and zeros that are arbitrarily close to the roots of $b_u(s) = 0$, when a small positive gain k is used. Thus, for sufficiently small gain k, the network input-output model is nonminimum phase as well as unstable if $H_u(s)$ is assumed to be unstable.

We note that results of the theorem may not apply in the very special case that $(H_1H_2 - H_3H_4) = 0$ or equivalently $(a_1a_2b_3b_4 - b_1b_2a_3a_4) = 0$. The distance-based condition $d_{ij} + d_{qn} \neq d_{in} + d_{qj}$ enforces that the relative degree of H_1H_2 and H_3H_4 are not equal, hence $(H_1H_2 - H_3H_4) \neq 0$ and the theorem result holds. ■

Proof of Theorem 9: The proof is the immediate result of the previous theorem. ■

Proof of Theorem 10: The model of this system is equivalent to the model of the network with PD-controlled HVDC line between input and output vertices, and equivalent parameters $k_p = k$ and $k_d = -kT_1$. In this case, k_p is positive and k_d is negative. From our analysis in theorem 2, we know that for either sufficiently large gain k_d or the gain k_p (equivalently sufficiently large k),

the zeros of the system are in OLHP except two of them, one at $s = 0$ and the other at $s = \frac{1}{T_1}$ which is in ORHP. ■

Proof of Theorem 11: The model of this system is equivalent to the model of the network with HVDC line, governing by lead compensator, between input and output vertices with equivalent parameters $T_1 = -0.5T_d$, $T_2 = 0.5T_d$, and $k = k$. In addition, T_2 is positive and T_1 is negative. From our analysis in theorem 3, we know that for either sufficiently large kT_d (i.e. either k or T_d is sufficiently large), and sufficiently small T_d, the zeros of the system are in OLHP except two of them, one at $s = 0$ and the other at $s = \frac{1}{T_1} = \frac{-1}{0.5T_d}$ which is in ORHP. More precisely, the condition sufficiently small T_d is not necessary, because based on the proof of the theorem 3, $\frac{T_d}{kT_d} = k^{-1}$ should be sufficiently small which means k should be sufficiently large. ■

Proof of Theorem 12: The model of this system is equivalent to the model of the network with HVDC line, governing by lead compensator, between input and output vertices with equivalent parameters $T_1 = -T_d$, $T_2 = T_2$, and $k = k$. In addition, T_2 is positive and T_1 is negative. From our analysis in theorem 3, we know that for either sufficiently large kT_d (i.e. either k or T_d is sufficiently large), and T_2 is sufficiently small (precisely sufficiently small $\frac{T_2}{kT_d}$), the zeros of the system are in OLHP except two of them, one at $s = 0$ and the other at $s = \frac{1}{T_1} = \frac{-1}{T_d}$ which is in ORHP. ■

3. Zeros Analysis for Detailed Power-System Models

3.1 Motivation and Scope

Recent advances in wide-area monitoring technology using synchrophasors have led to renewed interest in the design of wide-area controls for the bulk power transmission network, to shape small-signal and transient characteristics of the swing dynamics. Evaluation and design of such wide-area controls require analysis of the input-to-output characteristics of control channels. In particular, control designs for small-signal stability enhancement are often based on pole-zero characteristics of a linearized input-output model, see e.g. [29]. The poles (modes) of the swing dynamics, which are internal properties of the network (unrelated to the specific control channel considered), have been extensively characterized [30-31]. In contrast, there has been relatively little work on the zeros of the swing dynamics models.

The zeros of a linear model, or more explicitly its finite- and infinite- zero structure, are invariants to feedback and hence play a crucial role in analysis and design of controls. In particular, the zeros guide the structure of control designs, and place essential limits on control performance as well as the effort required for control. The reader is referred to the articles [32-33] for an overview of computation of linear system zeros, and the importance of zeros to control analysis and design. Precisely, the infinite-zero structure of the network decides the required dynamic complexity of the controller. Meanwhile, the presence of finite zeros in the right half plane (RHP), also known as non-minimum phase zeros, places essential limits on control performance and effort. For instance, as mentioned in [34], RHP zeros limit the maximum achievable bandwidth of HVDC controllers.

Other characteristics of the finite zeros, such as near pole-zero cancellations and poorly-damped left-half-plane (LHP) zeros, also influence control design and performance. Given this tight link between the zeros and control design, there is significant motivation to characterize the finite- and infinite- zero structure of linearized swing-dynamics models.

A few previous works have considered the computation and analysis of the zeros of the power system swing dynamics. The pioneering work by Martins et al. in [35] proposed methods for studying transfer function zeros in large-scale power system models. Authors of [36] have suggested creating an inverse system for the original system, whose poles are the zeros of the original system. Moreover, two methods for calculating a few dominant zeros which are close to a pre-specified point in the s-plane is suggested in the paper [36].

Same as the system poles, the system zeros change by changing the system operating point, since the system is non-linear. As reported in [37], a pair of complex conjugate RHP zeros can appear suddenly in real-time implementations, even though it may be absent in a set of input-output data at the present time. Moreover, the occasional presence of a zero close to a system mode can cause intermittent oscillation of the mode [37]. In summary, since the closed loop performance of the controllers highly depends on the presence of RHP zeros, the zeros should be monitored along with the estimation of system modes.

Authors of [38-39] have proposed four indicators for selecting the most appropriate remote feedback signals for designing auxiliary inter-area damping controllers on FACTS devices. It is mentioned that outputs which produce non-minimum phase zeros are undesirable, since by increasing the feedback gain, they may lead to gain instability. Therefore, as one indicator, remote

output signals with RHP zeros in the range of 0.1Hz to 2Hz are discarded from the candidate signals, even if they have higher controllability and observability indices comparing to the minimum-phase channels.

Analytical conditions were proposed in [40] for when RHP zeros can appear in general power system dynamics represented by classical angle stability models using swing equations. The work is extended in [41] where the effect of one control channel (especially HVDC line) on the finite zeros of the other input-output channels is characterized.

In this paper, we study the finite- and infinite- zero structures of detailed models of test power systems, focusing especially on the presence and impact of RHP transfer function zeros. Linearization of detailed swing-dynamics models are first undertaken using the commercial program Small-Signal Analysis Tool (SSAT) [42]. Then zeros are characterized for control channels of interest, for both the cases where the input and output are collocated (at the same bus) and where they are from different buses. Simulations include the study of zeros in two cases; PSS design and SVC damping controller design. The exciter control voltage reference and the SVC voltage control reference are the input locations, respectively. The outputs of interest are generator speed deviations, bus voltage magnitudes, bus voltage angles, bus angle differences, line current magnitudes, and line active power-flows. The studies show that in the case of traditional PSS design with local feedback, there is no RHP zero in the transfer function; however, the choice of remote output signals leads to non-minimum phase dynamics for most signals. Some numerical issues related to the zero computation are also highlighted. For example, it is shown that RHP zeros can be incorrectly calculated as LHP zeros or vice versa by using inaccurate power-flow solutions.

The rest of the paper is organized as follows. Section II describes the modeling and the algorithm used for calculating power system transfer function zeros. Case studies as well as observations are discussed in Section III. Section IV contains a brief conclusion and suggested future work.

3.2 Calculation of Transfer-Function Zeros: Fundamentals

A. Power system small signal modeling

Power system dynamics can be represented by Differential-Algebraic Equations (DAE) as follows.

$$\begin{aligned} \dot{x} &= f(x, y) \\ 0 &= g(x, y) \end{aligned} \qquad (1)$$

Here x and y are n- and 2m-dimensional vectors denoting the dynamic states and the network states, respectively.

For small signal analysis, the above non-linear equations can be linearized around an equilibrium point. Due to special structure of power systems, one may separately linearize the equations of each dynamic device and then aggregate all of them to obtain the overall system linearized DAE equations [15]. Each individual device can be modeled by the set of equations (2).

$$\begin{cases} \dot{x}_i = A_{d_i} x_i + B_{d_i} \Delta v \\ \Delta i_i = C_{d_i} x_i - D_{d_i} \Delta v \end{cases} \quad (2)$$

in which x_i is the state vector of the i^{th} device, i_i is the injected current into the network from the device, v is the vector of the network bus voltages.

The network states y in (2) contain the bus voltage information. They can be presented either in polar form (i.e., the bus voltage magnitudes and bus voltage angles) or in Cartesian form (i.e., voltage phasor real and imaginary parts). In this work, the latter Cartesian form which is employed in DSATools [42] is used.

Aggregating all equations of individual devices to obtain the overall system equations results in (3),

$$\begin{cases} \dot{x} = A_D x + B_D \Delta v \\ \Delta i = C_D x + D_D \Delta v \end{cases} \quad (3)$$

Here x is the state vector of the overall system which is made by stacking up all the x_i device state vectors together. $A_D, B_D, C_D,$ and D_D are block diagonal matrices built by assembling $A_i, B_i, C_i,$ and D_i associated with the individual devices.

The transmission system connects the dynamic devices together and is modeled by the algebraic equations in the form of (4).

$$\Delta i = Y_N \Delta v \quad (4)$$

In above equations, $A_D, B_D, C_D, D_D,$ and Y_N matrices are all real-valued and have dimensions $n \times n$, $n \times 2m$, $2m \times n$, $2m \times 2m$, and $2m \times 2m$, respectively, where n and m are the total number of states and number of system buses.

The overall state matrix of the system can be calculated by substituting (4) into (3) as follows [43].

$$A = A_D + B_D (Y_N - D_D)^{-1} C_D \quad (5)$$

This equation will be later used for simplifying the computation of transfer function zeros.

B. Transfer function zeros calculation

Let us consider the state equations of a general DAE system, i.e. a control channel or input-to-output map, as given in (6). A single-input single-output study of power system is of interest of this study.

$$\begin{aligned} E\dot{x}(t) &= A_c x(t) + B_c u(t) \\ y(t) &= C_c x(t) + D_c u(t) \end{aligned} \qquad (6)$$

In order to distinguish matrices with the same symbol, the index (subscript) *C* is used for control-channel (input-to-output system) matrices (i.e., input, output, and feedthrough matrices) and the index *D* for matrices derived from linearizing the DAE equations.

The zeros of the DAE system are defined as λ values in (7) such that the rank of the following matrix drops below its normal rank [44].

$$\begin{bmatrix} A_c - \lambda E & B_c \\ C_c & D_c \end{bmatrix} \qquad (7)$$

In the power systems model, the descriptor matrix E is the identity matrix of dimension of the system state matrix. Thus, for the rest of this work, the general descriptor matrix E will be substituted by the identity matrix I.

By substituting A_C from (5) into (7), we get that the zeros are λ values such that the following matrix (8) loses rank:

$$\begin{bmatrix} A_D + B_D (Y_N - D_D)^{-1} C_D - \lambda I & B_c \\ C_c & D_c \end{bmatrix} \qquad (8)$$

From a computational point of view, it would be preferable to avoid taking the inverse $(Y_N - D_D)$, since inverting such a large matrix is time consuming.

Based on the definition in (7), system zeros make the determinant of (8) equal to zero. Considering $\det\left(\begin{bmatrix} A_1 & A_2 \\ A_3 & A_4 \end{bmatrix}\right) = \det(A_4)\det(A_1 - A_2 A_4^{-1} A_3)$, the determinant of (8) can be written as (9):

$$\begin{aligned} &\det(D_c)\det((A_D + B_D (Y_N - D_D)^{-1} C_D - \lambda E) \\ &\qquad - B_c D_c^{-1} C_c) = 0 \end{aligned} \qquad (9)$$

Provided that $\det(D_c) \neq 0$, we have:

$$\det((A_D + B_D (Y_N - D_D)^{-1} C_D - \lambda E) - B_c D_c^{-1} C_c) = 0 \qquad (10)$$

Multiplying both sides of (10) by $\det(Y_N - D_D)$ and rearranging results in (11).

$$\begin{aligned} &\det(Y_N - D_D)\det(\underbrace{(A_D - B_D D_c^{-1} C_c - \lambda E)}_{n*n \text{ matrix}} - \\ &\qquad \underbrace{(-B_D)}_{n*2m \text{ matrix}} \underbrace{(Y_N - D_D)^{-1}}_{2m*2m \text{ matrix}} \underbrace{C_D}_{2m*n \text{ matrix}}) = 0 \end{aligned} \qquad (11)$$

The left side of (11) is the determinant of the matrix represented in (12).

$$\begin{bmatrix} A_D - B_c D_c^{-1} C_c - \lambda E & -B_D \\ C_D & Y_N - D_D \end{bmatrix} \qquad (12)$$

Finding transfer function zeros using (12) instead of (8) has the advantage of not requiring inversion of the matrix $(Y_N - D_D)$. For SISO systems, the *D* matrix is $1*1$, and hence easy to invert. However, for most power systems' input-output pairs, the feedthrough matrix is zero. Thus, (8) needs to be refined to a more general form. This can be done as follows.

For each λ value in (8), the vector $v = [w_1 \quad w_2]^T$ can be found such that (13) holds.

$$\begin{bmatrix} A_D + B_D (Y_N - D_D)^{-1} C_D - \lambda E & B_C \\ C_C & D_C \end{bmatrix} \begin{bmatrix} w_1 \\ w_2 \end{bmatrix} = \underline{0} \qquad (13)$$

To eliminate $(Y_N - D_D)^{-1}$ in the expression, the vector w_3 can be defined as (14).

$$(Y_N - D_D)^{-1} C_D w_1 = w_3 \qquad (14)$$

By substituting $B_D (Y_N - D_D)^{-1} C_D w_1$ with $B_D w_3$ and including $C_D w_1 - w_3 (Y_N - D_D) = 0$ into the sets of equations, the more efficient form (15) can be obtained.

$$\begin{bmatrix} A_D - \lambda E & B_C & B_D \\ C_C & D_C & 0 \\ C_D & 0 & -(Y_N - D_D) \end{bmatrix} \begin{bmatrix} w_1 \\ w_2 \\ w_3 \end{bmatrix} = \underline{0} \qquad (15)$$

Equation (15) is a generalized eigenvalue problem. For large-scale power systems, when only a few of zeros are of interest, the problem can be solved by means of efficient algorithms. We notice that the zeros analysis described here closely follows the development in [36].

By using (15) instead of (7), the number of calculated zeros increases by $2m$. The spurious additional zeros are found at infinity, i.e. the set of finite zeros remains the same.

3.3 Case Studies

The two-area test system described in [43] which is well known for displaying inter-area oscillations is considered for this study. The single line diagram of this system is depicted in Figure 6. Under high power transfers, it can be shown that the system has a poorly damped inter-area mode [15]. Traditional power system stabilizer (PSS) designs using local generator signals are discussed in detail in [17]-[19] for improving the damping of this inter-area mode.

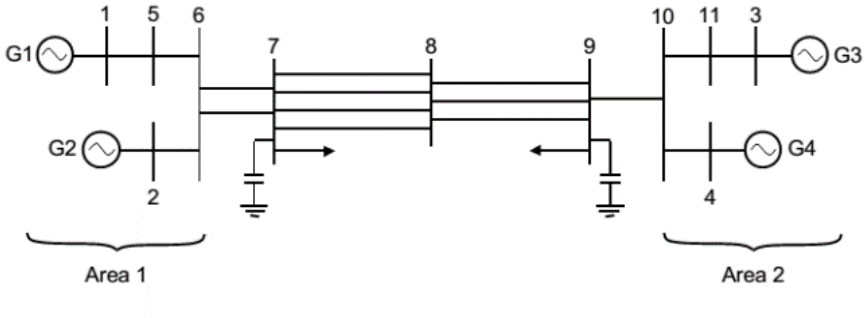

Figure 6. Two-area Kundur test system [28]

The study includes two parts. In the first part, the zeros for traditional PSS design as well as a design based on remote signals such as line current magnitude and active power are studied. The second part studies the presence of RHP zeros for SVC auxiliary damping control design for both local and remote channels.

A. PSS design

We are interested in the design of PSSs using both local and remote output signals. Suppose we consider the PSS design for Generator 1, then, the exciter control voltage reference V_{ref_1} is set to be the input. It is worth mentioning that the PSS of the generator at input location is disabled, whereas other generators are equipped with PSSs. The output is assumed to be taken from six choices of signals; generator speed deviation, bus voltage magnitude, bus voltage angle, bus angle difference, line current magnitude, and line active power

1) Generator speed signals

Table 1 shows the transfer function finite zeros when V_{ref_1} is the input and generator speed signals are outputs. In addition, the transfer function is found to have three infinite zeros (relative degree 3) for each output. The RHP zeros are bold in the table. Only for this case, all the finite zeros are shown. For other cases, for the sake of brevity, only RHP zeros and LHP zeros whose real value is greater than -10 are shown. It is interesting that there is no RHP zero for the traditional PSS design (i.e., while using generator 1 speed as the output). The same result is analytically shown in [40] where all the zeros of a local transfer function are in LHP for the classical generator model.

Table 1. System Zeros When Outputs are Generator Speed Signals

Output signal			
ω_1	ω_2	ω_3	ω_4
0.0000+0.0000i	0.0000+0.0000i	0.0000+0.0000i	0.0000+0.0000i
-0.5070+0.0000i	-0.4956+0.0000i	-0.5000+0.0000i	-0.5000+0.0000i
-0.5096+0.0000i	-0.5000+0.0000i	-0.5101+0.0000i	-0.5089+0.0000i
-0.5695+0.0000i	-0.5094+0.0000i	-0.5155+0.0000i	-0.5155+0.0000i
-0.7955+1.4030i	-1.3007+0.0000i	-1.6967+0.0000i	-1.6832+0.0000i
-0.7955-1.4030i	-2.3812+0.0000i	-2.5944+0.0878i	-2.2203+0.0000i

-2.3980+0.0000i	-3.3562+0.0000i	-2.5944-0.0878i	-3.0159+0.0000i
-3.1848+0.0000i	-3.4950+0.0000i	-3.4056+0.0000i	-3.4103+0.0000i
-4.3250+0.0698i	**0.1449+3.9114i**	-6.1043+0.0000i	-6.3516+0.0000i
-4.3250-0.0698i	**0.1449-3.9114i**	-0.8262+7.9503i	-0.6508+6.6966i
-0.6170+5.0710i	**3.9574+0.0000i**	-0.8262-7.9503i	-0.6508-6.6966i
-0.6170-5.0710i	-7.0017+0.0000i	-8.5763+0.3809i	**7.0961+0.0000i**
-0.7872+7.4944i	-0.7869+7.4923i	-8.5763-0.3809i	-0.9231+8.0755i
-0.7872-7.4944i	-0.7869-7.4923i	-1.0543+8.6834i	-0.9231-8.0755i
-8.7575+0.0000i	-8.7201+0.0000i	-1.0543-8.6834i	-8.2046+0.0000i
-10.301+0.0000i	-15.5660+7.3467i	**9.1771+0.0000i**	-10.7185+0.0000i
-14.378+8.8779i	-15.5660-7.3467i	-22.878+3.9125i	-21.429+4.4108i
-14.3786-8.8779i	-20.4752+0.0000i	-22.8787-3.9125i	-21.4296-4.4108i
-20.8717+0.0000i	-13.5504+17.4012i	-23.1703+4.7750i	-22.9932+4.2642i
-20.5606+4.2459i	-13.5504-17.4012i	-23.1703-4.7750i	-22.9932-4.2642i
-20.5606-4.2459i	-22.4630+4.4329i	-25.0000+0.0000i	-25.0000+0.0000i
-22.4635+4.4318i	-22.4630-4.4329i	-25.0000+0.0000i	-25.0000+0.0000i
-22.4635-4.4318i	-25.0000+0.0000i	-28.7828+0.0000i	-9.0491+23.3955i
-28.7530+0.0000i	-25.0000+0.0000i	-1.6847+28.8457i	-9.0491-23.3955i
-29.3360+0.0000i	-28.7519+0.0000i	-1.6847-28.8457i	-28.7658+0.0000i
-31.5719+0.0000i	-30.8339+0.0000i	-30.2531+0.0000i	-30.4904+0.0000i
-32.7039+0.0000i	-32.9218+0.2756i	-32.4729+0.0000i	-32.8641+0.0000i
-33.3012+0.0000i	-32.9218-0.2756i	-33.5373+0.0000i	-33.8350+0.0000i
-35.4668+0.0000i	-34.5527+0.0000i	-38.7999+0.2745i	-35.8535+0.0000i
-37.2776+0.0000i	-37.2689+0.0000i	-38.7999-0.2745i	-38.7657+0.0000i
-51.8299+0.0000i	-51.8306+0.0000i	-51.4542+0.2405i	-51.3925+0.0000i
-52.3609+0.0000i	-52.7310+0.0000i	-51.4542-0.2405i	-52.1878+0.0000i
-52.8413+0.0000i	-53.5758+0.0000i	-54.2328+0.0000i	-53.9522+0.0000i
-66.6666+0.0000i	-66.6667+0.0000i	-66.6667+0.0000i	-66.6667+0.0000i

If any other generator speed is used as the output for the transfer function (which would then be the input for the generator 1 PSS design), the transfer function has RHP zeros some real and some complex conjugate. It is interesting that this is different from the results in [40], where there is no RHP zero if there is only one path between the input and the output nodes.

It is noted that similar results are obtained when other generators are examined; showing no RHP zero for local output and having real and complex conjugate zeros for remote speed signals.

It should be mentioned that for all generator speed signals, one zero at origin is found. This is because of the fact that the generator speed signal is basically the time-derivative of the respective generator rotor angle. This corresponds to an *s* in Laplace domain (i.e., a zero at origin).

2) Bus voltage magnitude signals

Table 2 shows the zeros of the input V_{ref_1} paired with bus voltage magnitudes as outputs. In this case, the transfer function has exactly two RHP zeros for each choice of voltage magnitude signals V_1 through V_{11}.

Table 2. System Zeros When Outputs are Bus Voltage Magnitude Signals

Output signal			
V_1	V_2	V_3	V_4
0.0002+0.0083i	**0.0120+0.0000i**	**0.0130+0.0000i**	**0.0128+0.0000i**
0.0002-0.0083i	**0.2649+0.0000i**	-2.1034+0.3804i	**1.9520+0.0000i**
-3.4633+0.2021i	-3.4095+0.0958i	-2.1034-0.3804i	-0.2845+5.0235i
-3.4633-0.2021i	-3.4095-0.0958i	**2.8555+0.0000i**	-0.2845-5.0235i
-0.1359+4.4406i	-0.1567+4.7821i	-0.2699+5.1795i	-0.8143+7.7220i
-0.1359-4.4406i	-0.1567-4.7821i	-0.2699-5.1795i	-0.8143-7.7220i
-0.9314+7.3892i	-0.8063+7.4952i	-0.8851+7.7263i	-0.4255+7.9074i
-0.9314-7.3892i	-0.8063-7.4952i	-0.8851-7.7263i	-0.4255-7.9074i
-0.7833+7.5091i	-0.3336+7.8854i	-8.0251+0.4586i	-
-0.7833-7.5091i	-0.3336-7.8854i	-8.0251-0.4586i	-
-	-	-0.4176+8.0459i	-
-	-	-0.4176-8.0459i	-

V_5	V_6	V_7	V_8
0.0002+0.0088i	**0.0002+0.0105i**	**0.0002+0.0096i**	**0.0001+0.0107i**
0.0002-0.0088i	**0.0002-0.0105i**	**0.0002-0.0096i**	**0.0001-0.0107i**
-3.4302+0.1647i	-3.4043+0.1118i	-3.3965+0.1089i	-3.3686+0.1019i
-3.4302-0.1647i	-3.4043-0.1118i	-3.3965-0.1089i	-3.3686-0.1019i
-0.1556+4.5615i	-0.1498+4.8921i	-0.1285+5.0348i	-0.0712+5.3521i
-0.1556-4.5615i	-0.1498-4.8921i	-0.1285-5.0348i	-0.0712-5.3521i
-0.8125+7.5039i	-0.8087+7.5046i	-0.8149+7.5120i	-0.8370+7.5371i
-0.8125-7.5039i	-0.8087-7.5046i	-0.8149-7.5120i	-0.8370-7.5371i
-0.8036+7.6524i	-0.5157+7.9446i	-0.4973+7.9255i	-0.4463+7.8745i
-0.8036-7.6524i	-0.5157-7.9446i	-0.4973-7.9255i	-0.4463-7.8745i

V_9	V_{10}	V_{11}
0.0084+0.0485i	**0.0223+0.0000i**	**0.0513+0.0000i**
0.0084-0.0485i	**0.6170+0.0000i**	**1.7543+0.0000i**
-0.1797+5.0358i	-0.4656+4.7449i	-2.2109+0.2490i
-0.1797-5.0358i	-0.4656-4.7449i	-2.2109-0.2490i
-0.8678+7.6559i	-0.8519+7.6841i	-0.7248+4.8127i
-0.8678-7.6559i	-0.8519-7.6841i	-0.7248-4.8127i
-0.4095+7.9179i	-0.4239+7.9716i	-0.8621+7.7287i
-0.4095-7.9179i	-0.4239-7.9716i	-0.8621-7.7287i
-	-	-0.3925+8.0357i
-	-	-0.3925-8.0357i
-	-	-8.3553+0.3835i
-	-	-8.3553-0.3835i

As can be seen from Table 2, for some outputs such as V_1, there is a pair of conjugate zeros which are very small in magnitude. Now, naturally, a question arises as to whether these zeros are caused by numerical issues or they are genuine. Because of not using the relative rotor angles in small signal modeling, an eigenvalue at origin is expected. Depending on the power flow solution mismatch, this eigenvalue will be calculated somewhere around the origin. For instance, in the two-area system used in this study, this eigenvalue is calculated as $\lambda = +0.082$ and $\lambda = -0.000031 \pm 0.00902i$ when power flow mismatch is chosen as $1MW$ and $0.001MW$, respectively.

This suggests that the zeros close to origin might be inaccurate. The root locus analysis proposes that by increasing the feedback gain, the poles of the closed-loop system approaches to the system zeros. Thus, in order for validating the zeros calculation, one may perform the root locus analysis either by manipulating the effect of feedback in the system state matrix or by adding the appropriate feedback into the model. Although investigation on this example shows that the poles of closed-loop system approaches to the (very small) zeros, this is not a valid approach, since both of the open-loop and closed-loop systems are derived with the same level of power flow accuracy.

A closer scrutiny reveals that the accuracy of power flow solution highly effects the zeros calculation, especially those which are close to the origin. Table 3 shows the calculated zeros for some cases with trivial zeros. Two values for power flow mismatch are considered.

Table 3. Effect of Power Flow Accuracy on Calculated Zeros

Power flow mismatch (MW)	Output signals			
	V_1	V_2	V_3	$\delta_1 - \delta_5$
1 (default value)	0.0830	0.3173	$-0.0086 \pm 0.0942i$	0.0758 -0.0708
0.001	$0.0002 \pm 0.0083i$	0.0120	0.0130	$-0.0002 \pm 0.0294i$

It can be observed from Table 3 that by increasing the power flow solution accuracy, some RHP zeros move into LHP, and vice versa. Moreover, some real-valued zeros have disappeared and two new oscillatory zeros emerge, and vice versa. Since the power mismatch $0.001MW$ is the smallest value feasible in the software used, further investigation on the role of power flow solution accuracy is left as an open question.

3) Bus voltage angle signals

Table 4 shows the system zeros when bus voltage angles are set as outputs (even for the local bus voltage δ_1). . It can be seen that a real-valued RHP zero is present when the output is any of the bus voltage angles. For some buses, complex conjugate zeros are observed as well.

4) Bus voltage angle difference signals

The system zeros when the input V_{ref_1} is paired with some bus voltage angle differences is shown in Table 5. The choices include connected buses such as Buses 1 and 5, and also buses which are across the system such as Buses 6 and 10. Same as for the choice of bus voltage phase angles, real-valued RHP zeros can be observed for all choices.

It is notable that similar to the case where bus voltage magnitude signals were chosen as output, very small zeros are observed in this case.

Table 4. System Zeros When Outputs are Bus Voltage Angle Signals

Output signal			
δ_1	δ_2	δ_3	δ_4
-0.6113+3.0970i	-0.3153+3.5868i	-0.9696+7.8666i	-0.4158+6.9725i
-0.6113-3.0970i	-0.3153-3.5868i	-0.9696-7.8666i	-0.4158-6.9725i
5.5692+0.0000i	**7.1682+0.0000i**	-0.6218+8.1561i	-0.8402+7.9783i
-1.0439+6.1866i	-0.7892+7.4895i	-0.6218-8.1561i	-0.8402-7.9783i
-1.0439-6.1866i	-0.7892-7.4895i	-8.5869+2.3532i	-9.5782+2.0608i
-0.7868+7.4974i	**0.2248+10.0517i**	-8.5869-2.3532i	-9.5782-2.0608i
-0.7868-7.4974i	**0.2248-10.0517i**	**5.3558+8.1234i**	**3.1768+9.6458i**
-	-	**5.3558-8.1234i**	**3.1768-9.6458i**
-	-	**19.7192+0.0000i**	**11.3941+0.0000i**

δ_5	δ_6	δ_7	δ_8
-0.5241+3.3261i	-0.3840+3.6335i	-0.3812+3.7340i	-0.3661+4.0696i
-0.5241-3.3261i	-0.3840-3.6335i	-0.3812-3.7340i	-0.3661-4.0696i
5.5325+0.0000i	**5.9555+0.0000i**	**5.9278+0.0000i**	**5.9447+0.0000i**
-1.1214+6.7158i	-0.7962+7.4878i	-0.7974+7.4902i	-0.8023+7.5003i
-1.1214-6.7158i	-0.7962-7.4878i	-0.7974-7.4902i	-0.8023-7.5003i
-0.7866+7.5005i	-0.8373+8.2490i	-0.8313+8.2495i	-0.8146+8.2563i
-0.7866-7.5005i	-0.8373-8.2490i	-0.8313-8.2495i	-0.8146-8.2563i

δ_9	δ_{10}	δ_{11}
0.0270+6.2705i	-0.0804+7.0988i	-0.9341+7.7698i
0.0270-6.2705i	-0.0804-7.0988i	-0.9341-7.7698i
7.5913+0.0000i	-0.7919+7.8317i	-0.5208+8.0270i
-0.8120+7.6956i	-0.7919-7.8317i	-0.5208-8.0270i
-0.8120-7.6956i	**0.4936+8.6195i**	-8.9372+2.6837i
-0.4680+8.4895i	**0.4936-8.6195i**	-8.9372-2.6837i
-0.4680-8.4895i	**8.8036+0.0000i**	**2.9845+8.8676i**
-	-	**2.9845-8.8676i**
-	-	**11.6352+0.0000i**

Table 5. System Zeros When Outputs are Bus Voltage Angle Difference Signals

Output signal			
$\delta_1-\delta_5$	$\delta_5-\delta_6$	$\delta_6-\delta_7$	$\delta_7-\delta_8$
-0.0002+0.0294i	**0.0414+0.0000i**	-0.0021+0.0721i	**0.0480+0.0000i**
-0.0002-0.0294i	**4.2376+0.0000i**	-0.0021-0.0721i	**5.7816+0.0000i**
-0.3191+4.9056i	-0.3763+4.9756i	**6.8704+0.0000i**	-0.7719+7.4487i
-0.3191-4.9056i	-0.3763-4.9756i	-0.7722+7.4491i	-0.7719-7.4487i
5.8482+0.0000i	-0.7880+7.4944i	-0.7722-7.4491i	-0.8952+8.2094i
-0.7878+7.4942i	-0.7880-7.4944i	-0.9378+8.2228i	-0.8952-8.2094i
-0.7878-7.4942i	-	-0.9378-8.2228i	-

$\delta_8-\delta_9$	$\delta_9-\delta_{10}$	$\delta_{10}-\delta_{11}$	$\delta_4-\delta_{10}$
-0.0003+0.0357i	-0.0008+0.0481i	**0.0671+0.0000i**	**0.0708+0.0000i**
-0.0003-0.0357i	-0.0008-0.0481i	**5.1461+0.0000i**	**4.6575+0.0000i**
4.3942+0.0000i	**4.0368+0.0000i**	-0.8440+7.9072i	-0.7786+6.7901i
-0.7714+7.4483i	-0.7713+7.4481i	-0.8440-7.9072i	-0.7786-6.7901i
-0.7714-7.4483i	-0.7713-7.4481i	-8.6054+0.5018i	-0.8937+8.1125i
-0.8394+8.1864i	-0.8256+8.1796i	-8.6054-0.5018i	-0.8937-8.1125i
-0.8394-8.1864i	-0.8256-8.1796i	-0.5664+8.6617i	-
-8.7935+0.1514i	-	-0.5664-8.6617i	-
-8.7935-0.1514i	-	-	-

5) Line currents signals

Table 6 shows the system zeros when the magnitude of line current signals are of interest. For each choice of line, at least there is one RHP zero. Moreover, all RHP zeros are real-valued.

6) Line active power signals

The line active power signal is another good candidate to examine, since inter-area oscillations are clearly seen in line flows. Table 7 shows transfer function zeros when line active power signals are of interest. Similar to line current and bus angle difference cases, at least one RHP zero is observed for each choice.

Table 6. System Zeros when Outputs are Line Currents Signals

Output signal			
I_{1-5}	I_{5-6}	I_{6-7}	I_{7-8}
-0.0024+0.0634i	**0.0833+0.0000i**	-0.0230+0.1509i	**0.0553+0.0000i**
-0.0024-0.0634i	-1.1529+0.1324i	-0.0230-0.1509i	**3.9888+0.0000i**
-1.1626+0.0749i	-1.1529-0.1324i	**1.0954+0.0000i**	-0.7754+7.4566i
-1.1626-0.0749i	**1.4836+0.0000i**	-1.3865+0.9526i	-0.7754-7.4566i
1.5280+0.0000i	-0.4991+5.0492i	-1.3865-0.9526i	-0.8167+8.1857i

-0.4973+5.0475i	-0.4991-5.0492i	-2.1861+0.2355i	-0.8167-8.1857i
-0.4973-5.0475i	-0.7876+7.4945i	-2.1861-0.2355i	-8.6656+0.3392i
-0.7876+7.4945i	-0.7876-7.4945i	-3.3390+0.3354i	-8.6656-0.3392i
-0.7876-7.4945i	-	-3.3390-0.3354i	-
-	-	-0.7826+7.4708i	-
-	-	-0.7826-7.4708i	-
-	-	-0.7129+8.1309i	-
-	-	-0.7129-8.1309i	-

I_{8-9}	I_{9-10}	I_{10-11}	I_{4-10}
-0.0004+0.0381i	-0.0005+0.0515i	**0.0701+0.0000i**	**0.0853+0.0000i**
-0.0004-0.0381i	-0.0005-0.0515i	**5.9969+0.0000i**	**4.7032+0.0000i**
3.5574+0.0000i	**5.3437+0.0000i**	-0.8411+7.9246i	-0.7259+6.7899i
-0.7752+7.4560i	-0.7531+7.4160i	-0.8411-7.9246i	-0.7259-6.7899i
-0.7752-7.4560i	-0.7531-7.4160i	-8.5000+0.4944i	-0.8968+8.0969i
-0.8006+8.1760i	-0.8921+8.1627i	-8.5000-0.4944i	-0.8968-8.0969i
-0.8006-8.1760i	-0.8921-8.1627i	-0.7306+8.7083i	-
-8.5502+0.1820i	-	-0.7306-8.7083i	-
-8.5502-0.1820i	-	-	-

7) Summary

Traditional PSS design uses local machine speed signal or local machine accelerating power signal as feedback input signals. However, if non-traditional signals such as active power-flow on tie-lines are used, Tables I to VII show that the use of non-traditional signals can introduce right half plane zeros in almost all the cases. Potential numerical issues in the case of analyzing remote bus voltage magnitudes in Table II require further scrutiny. The results in this section emphasize abundant caution in the use of remote as well as local non-traditional signals for feedback control designs in PSS units.

Table 7. System Zeros when Outputs are Line Active Power Signals

Output signal			
P_{1-5}	P_{5-6}	P_{6-7}	P_{7-8}
0.0790+0.0000i	**0.0752+0.0000i**	**0.0990+0.0000i**	**0.0623+0.0000i**
-0.7961+1.4114i	**1.3026+0.0000i**	-0.4879+3.1158i	**3.1117+0.0000i**
-0.7961-1.4114i	-0.4876+4.9638i	-0.4879-3.1158i	-3.9824+0.6324i
-4.3219+0.0962i	-0.4876-4.9638i	-3.3707+0.1893i	-3.9824-0.6324i
-4.3219-0.0962i	-0.7870+7.4941i	-3.3707-0.1893i	-0.7791+7.4643i
-0.6177+5.0712i	-0.7870-7.4941i	-0.7898+7.4833i	-0.7791-7.4643i
-0.6177-5.0712i	-8.4346+0.2011i	-0.7898-7.4833i	-0.7766+8.1711i
-0.7872+7.4944i	-8.4346-0.2011i	-0.6420+8.0768i	-0.7766-8.1711i
-0.7872-7.4944i	-	-0.6420-8.0768i	-8.4316+0.1998i
-	-	-	-8.4316-0.1998i

P_{8-9}	P_{9-10}	P_{10-11}	P_{4-10}
-0.0005+0.0381i	-0.0002+0.0497i	**0.0738+0.0000i**	**0.0845+0.0000i**
-0.0005-0.0381i	-0.0002-0.0497i	-0.8118+7.9545i	-0.6505+6.6962i
3.1856+0.0000i	-0.7266+7.3788i	-0.8118-7.9545i	-0.6505-6.6962i
-4.0275+0.5929i	-0.7266-7.3788i	-1.2341+8.6904i	**7.1103+0.0000i**
-4.0275-0.5929i	-0.9875+8.1146i	-1.2341-8.6904i	-0.9232+8.0754i
-0.7789+7.4638i	-0.9875-8.1146i	**19.9993+0.0000i**	-0.9232-8.0754i
-0.7789-7.4638i	**10.7859+0.0000i**	**28.3275+22.9337i**	-9.0190+23.4422i
-0.7796+8.1725i	-1.8377+29.9188i	**28.3275-22.9337i**	-9.0190-23.4422i
-0.7796-8.1725i	-1.8377-29.9188i	-	-
-8.4456+0.2236i	-	-	-
-8.4456-0.2236i	-	-	-

B. SVC auxilary control design

SVCs are mainly used for dynamic voltage regulation of key buses in the power system. In this section, we study the design of supplementary small-signal stability control that introduces an additional stabilization loop in SVC by using a remote input signal. By employing remote signals, the inter-area oscillations can be mitigated as shown in many papers (e.g. [38]). In [48], it is analytically shown that depending on the system load level, the use of remote generator speed signals for SVC control can improve the damping of inter-area and or local modes in a simple power system.

In this section, an SVC with the capacity of $\pm 200\text{MVAR}$, installed at Bus 8, is considered. Here the design of SVC auxiliary control is of interest, and the SVC voltage reference (i.e., V_{ref} of SVC) is set as the input. Note that the SVC voltage controller is not disabled and local bus voltage regulation is the primary control objective of the SVC. Three sets of outputs are considered; generator speeds, bus voltage magnitudes, and bus voltage angle difference signals for supplementary stability control.

1) Generator speed signals

Table 8 shows the system zeros when generator speed signals are selected as remote output signals. The zeros at origin are also observed in this case. It is interesting that except for generator 2, other generator speed signals do not show non-minimum phase behavior, and can be considered as potential choices for SVC damping control.

Table 8. System Zeros when Outputs are Generator Speed Signals

Output signal			
ω_1	ω_2	ω_3	ω_4
0.0000+0.0000i	0.0000+0.0000i	0.0000+0.0000i	0.0000+0.0000i
-2.2693+0.4115i	**0.1545+4.1356i**	-2.9257+0.3957i	-3.1247+0.2760i
-2.2693-0.4115i	**0.1545-4.1356i**	-2.9257-0.3957i	-3.1247-0.2760i
-0.0375+4.0367i	-0.0577+6.6158i	-0.4141+5.2752i	-0.6537+5.0079i
-0.0375-4.0367i	-0.0577-6.6158i	-0.4141-5.2752i	-0.6537-5.0079i

-0.7794+7.5147i	-0.7814+7.5152i	-0.7895+7.4504i	-0.0656+7.1225i
-0.7794-7.5147i	-0.7814-7.5152i	-0.7895-7.4504i	-0.0656-7.1225i
-1.5731+8.0532i	-	-1.7624+8.0436i	-0.7723+7.4363i
-1.5731-8.0532i	-	-1.7624-8.0436i	-0.7723-7.4363i
-8.8017+1.0061i	-	-9.7884+2.2522i	-
-8.8017-1.0061i	-	-9.7884-2.2522i	-

2) Bus voltage magnitude signals

Although the voltage magnitude signal of Bus 8 is already used as feedback signal in SVC voltage control loop, looking at bus voltage magnitude signals reveals a problem that might occur for calculation of infinite zeros.

Although (15) is the extended version of (7), sometimes, some of the calculated zeros by these equations are different. For example, let us consider a case when the output is considered as voltage magnitude of Bus 9 (see Table 9). Then, using (15), two zeros at $-1.2545*10^{9}$ and $1.2545*10^{9}$ are obtained, whereas using (7), two zeros at $35.90 + i\,3.96*10^{7}$ and $35.90 - i\,3.96*10^{7}$ are obtained. All other zeros are exactly same.

By investigating the transfer function relative degree, it is observed that the matrix multiplications $C_c B_c = 0$ and $C_c A_c B_c \neq 0$ hold. Thus, the transfer function relative degree is 2 [49]. It means that there are two infinite zeros. Further investigation shows that this is true when other bus voltage magnitude signals are considered as output signal. In other words, the two zeros calculated as large real or imaginary numbers are infinite zeros and due to numerical issues these are calculated as large finite values.

It can be seen from Table 9 that except for the buses close to generators, other bus voltage magnitude signals (those which are close to SVC as well) have very small zeros, and the Bus 9 has no RHP zeros at all. As mentioned earlier, these small zeros are very sensitive to power flow solution and might be at LHP or at origin. Further investigation of the effect of equilibrium point accuracy should be performed for this case as well.

Table 9. System Zeros when Outputs are Bus Voltage Magnitude Signals as Outputs

Output signal			
V_1	V_2	V_3	V_4
0.0061+0.0000i	**0.0008+0.0029i**	**0.0054+0.0000i**	**0.0100+0.0000i**
1.5312+0.0000i	**0.0008-0.0029i**	-1.9674+0.4413i	**1.6208+0.0000i**
-1.7178+0.3297i	**0.7243+0.0000i**	-1.9674-0.4413i	-0.1951+4.4786i
-1.7178-0.3297i	-0.1787+4.5440i	**3.0291+0.0000i**	-0.1951-4.4786i
-0.1519+4.5177i	-0.1787-4.5440i	-0.2343+4.5199i	-0.6671+7.2737i
-0.1519-4.5177i	-0.6837+7.2404i	-0.2343-4.5199i	-0.6671-7.2737i

-0.6206+7.3003i	-0.6837-7.2404i	-0.6242+7.2964i	-0.7715+7.4918i
-0.6206-7.3003i	-0.7783+7.5115i	-0.6242-7.2964i	-0.7715-7.4918i
-7.3130+0.5429i	-0.7783-7.5115i	-7.3262+0.7709i	$4.9839*10^{7}$
-7.3130-0.5429i	$(0.0+4.9365i)*10^{7}$	-7.3262-0.7709i	$-4.9839*10^{7}$
-0.7793+7.5107i	$(0.0-4.9365i)*10^{7}$	-0.7621+7.4870i	-
-0.7793-7.5107i	-	-0.7621-7.4870i	-
$3.7437*10^{7}$	-	(0.0+2.6407i)$*10^{7}$	-
$-3.7437*10^{7}$	-	(0.0-2.6407i)$*10^{7}$	-

V_5	V_6	V_7	V_8
0.0322+0.0000i	**0.0045+0.0000i**	**0.0023+0.0000i**	**0.0002+0.0024i**
0.0872+0.0000i	-0.1981+4.5668i	-0.1961+4.5502i	**0.0002-0.0024i**
-1.9618+0.2319i	-0.1981-4.5668i	-0.1961-4.5502i	-0.1724+4.5117i
-1.9618-0.2319i	-0.6803+7.2695i	-0.7027+7.2861i	-0.1724-4.5117i
-0.1763+4.5876i	-0.6803-7.2695i	-0.7027-7.2861i	-0.7363+7.3006i
-0.1763-4.5876i	-0.7784+7.5108i	-0.7782+7.5106i	-0.7363-7.3006i
-0.6279+7.2451i	-0.7784-7.5108i	-0.7782-7.5106i	-0.7782+7.5104i
-0.6279-7.2451i	$(0.0+4.5940i)*10^{7}$	$7.4334*10^{7}$	-0.7782-7.5104i
-0.7789+7.5111i	$(0.0-4.5940i)*10^{7}$	$-7.4334*10^{7}$	$3.2375*10^{15}$
-0.7789-7.5111i	-	-	-
-8.1137+0.6596i	-	-	-
-8.1137-0.6596i	-	-	-
$4.9944*10^{7}$	-	-	-
$-4.9944*10^{7}$	-	-	-

V_9	V_{10}	V_{11}
-0.0002+0.0032i	**0.0452+0.0218i**	**0.0076+0.0000i**
-0.0002-0.0032i	**0.0452-0.0218i**	**1.2008+0.0000i**
-0.1644+4.4778i	-0.1628+4.4195i	-2.1421+0.2752i
-0.1644-4.4778i	-0.1628-4.4195i	-2.1421-0.2752i
-0.6972+7.2996i	-0.6696+7.2856i	-0.2239+4.3826i
-0.6972-7.2996i	-0.6696-7.2856i	-0.2239-4.3826i
-0.7687+7.5017i	-0.7682+7.4953i	-0.6287+7.2639i
-0.7687-7.5017i	-0.7682-7.4953i	-0.6287-7.2639i
-8.4335+0.0998i	$+9.2895*10^{7}$	-0.7674+7.4868i
-8.4335-0.0998i	$-9.2895*10^{7}$	-0.7674-7.4868i
$1.2545*10^{9}$	-	-8.2053+0.8321i
$-1.2545*10^{9}$	-	-8.2053-0.8321i
-	-	$(0.0+4.9938i)*10^{7}$
-	-	$(0.0-4.9938i)*10^{7}$

3) Bus voltage angle difference signals

System zeros when the output choice is bus voltage angle difference is presented in Table 10. As can be seen from Table 10, the problem of very small zeros appears in SVC case as well. In fact, angle difference signals which are across the system such as $\delta_6 - \delta_{10}$ and $\delta_7 - \delta_9$ show no non-minimum phase behavior, and can be considered as suitable candidates for SVC inter-area damping control signals.

Table 10. System Zeros when Outputs are Bus Voltage Angle Difference Signals

Output signal			
$\delta_6 - \delta_7$	$\delta_7 - \delta_8$	$\delta_8 - \delta_9$	$\delta_9 - \delta_{10}$
0.0763+0.0000i	**0.0219+0.0000i**	**0.0002+0.0124i**	**0.0114+0.0000i**
1.6566+1.7819i	-4.2226+1.7100i	**0.0002-0.0124i**	-3.3482+4.5436i
1.6566-1.7819i	-4.2226-1.7100i	-2.4619+5.2970i	-3.3482-4.5436i
-2.4933+0.0735i	-0.6553+7.0296i	-2.4619-5.2970i	-0.7609+6.9463i
-2.4933-0.0735i	-0.6553-7.0296i	-0.8869+6.9515i	-0.7609-6.9463i
-0.6443+7.2152i	-0.7916+7.5341i	-0.8869-6.9515i	-0.7867+7.5372i
-0.6443-7.2152i	-0.7916-7.5341i	-0.7823+7.5376i	-0.7867-7.5372i
-0.7963+7.5229i	-7.6780+1.0180i	-0.7823-7.5376i	$2.2404 * 10^8$
-0.7963-7.5229i	-7.6780-1.0180i	-	-
-8.7449+0.1508i	-	-	-
-8.7449-0.1508i	-	-	-
$(-0.0-3.0288i) * 10^8$	-	-	-
$(-0.0-3.0288i) * 10^8$	-	-	-

$\delta_6 - \delta_{10}$	$\delta_7 - \delta_9$	$\delta_{10} - \delta_{11}$	$\delta_4 - \delta_{10}$
0.0002+0.0110i	**0.0003+0.0082i**	**0.0134+0.0000i**	**0.0250+0.0000i**
0.0002-0.0110i	**0.0003-0.0082i**	-0.5649+5.7940i	-1.1930+4.7734i
-3.5206+4.8233i	-3.0331+5.1608i	-0.5649-5.7940i	-1.1930-4.7734i
-3.5206-4.8233i	-3.0331-5.1608i	-4.4238+5.2157i	-0.7735+7.4248i
-0.7662+6.9473i	-0.8172+6.9399i	-4.4238-5.2157i	-0.7735-7.4248i
-0.7662-6.9473i	-0.8172-6.9399i	-0.7862+7.4568i	**0.4709+7.6466i**
-0.7864+7.5371i	-0.7846+7.5374i	-0.7862-7.4568i	**0.4709-7.6466i**
-0.7864-7.5371i	-0.7846-7.5374i	$(-0.0+3.4376i) * 10^8$	-8.4812+0.1474i
-	-	$(-0.0-3.4376i) * 10^8$	-8.4812-0.1474i
-	-	-	$(-0.0+3.4003i) * 10^8$
-	-	-	$(-0.0-3.4003i) * 10^8$

3.4. Discussion

The paper studies the presence of non-minimum phase dynamics in the design of wide-area damping controllers. Two different case-studies are considered. In the first one, the zeros for PSS design based on both local and remote signals are examined. The second case studies the non-minimum phase zeros for SVC damping control design. For some input-output channels, numerical issues are observed. The effect of power-flow accuracy on the calculation of zeros which are very close to the origin requires further investigation. Moreover, it was shown that in some cases, infinite zeros appear as large finite RHP zeros which lead to misinterpretation of RHP zeros. For the SVC case, appropriate output signal candidates are suggested from the absence of RHP zeros.

4. Conclusions

This project has characterized the input-output properties of the swing dynamics of the bulk power grid, with the aim of supporting modeling, analysis, and control design of today's renewables rich and power-electronics-enabled grid. Two main studies have been undertaken: first, the dependence of control channels in the grid on the tuning of remote control systems has been explored for the classical model for the swing dynamics, with numerous graph-theoretic results obtained. Second, the analysis of control channels has been undertaken for detailed models of the swing dynamics, via simulations. Both studies show that transfer-function properties (e.g., zeros) depend on the structure of the grid in a sophisticated way. Understanding this dependence can facilitate modeling and design of the bulk grid, for the purpose of controller design.

References

[1] Anderson, Paul M., and Aziz A. Fouad. *Power System Control and Stability.* John Wiley and Sons, 2008.

[2] Korba, Petr, et al. “Combining forces to provide stability." *ABB Review 3* (2007): 34-38.

[3] Ulbig, Andreas, Theodor S. Borsche, and Goran Andersson. "Analyzing Rotational Inertia, Grid Topology and their Role for Power System Stability." *IFAC-PapersOnLine* 48.30 (2015): 541-547.

[4] Bose, Anjan. "Smart transmission grid applications and their supporting infrastructure." *Smart Grid, IEEE Transactions on* 1.1 (2010): 11-19.

[5] Chakrabortty, Aranya, and Pramod P. Khargonekar. "Introduction to wide-area control of power systems." American Control Conference (ACC), 2013. IEEE, 2013.

[6] K. Koorehdavoudi et al, “Input-output characteristics of the power transmission network’s swing dynamics,” to appear in Decision and Control (CDC), 2016 IEEE 55th Annual Conference on. IEEE, 2016 (also an extended version is available at www.eecs.wsu.edu/∼kkoorehd).

[7] Schrader, Cheryl B., and Michael K. Sain. “Research on system zeros: a survey." *International Journal of Control*, 50.4 (1989): 1407-1433.

[8] N. Martins, H. J. C. P. Pinto, and L. T. G. Lima, “Efficient methods for finding transfer function zeros of power systems," *IEEE Transactions on Power Systems*, vol. 7, no. 3, Aug. 1992.

[9] C. W. Taylor, S. Lefebvre, "HVDC controls for system dynamic performance", IEEE Trans on Power System, vol. 6, no. 2, pp. 743-752, May 1991.

[10] Huang Ying, Xu Zheng, "HVDC supplementary controller based on synchronized phasor measurement units", Proceedings of CSEE, vol. 24, no. 9, pp. 7-12, September 2004.

[11] Briegel, Benjamin, et al. “On the zeros of consensus networks." Decision and Control and European Control Conference (CDC-ECC), 2011 50th IEEE Conference on. IEEE, 2011.

[12] Herman, Ivo, Dan Martinec, and Michael Sebek. “Zeros of transfer functions in networked control with higher-order dynamics." *Proceedings of the 19th IFAC World Congress*. 2014.

[13] Abad Torres, Jackeline, and Sandip Roy. “Graph-theoretic characterisations of zeros for the inputâ€“output dynamics of complex network processes." *International Journal of Control* 87.5 (2014): 940-950.

[14] Abad Torres, Jackeline, and Sandip Roy. “Graph-theoretic analysis of network inputâ€“output processes: Zero structure and its implications on remote feedback control." *Automatica* 61 (2015): 73-79.

[15] Abad Torres, Jackeline, and Sandip Roy. “A two-layer transformation for characterizing the zeros of a network input-output dynamics." Decision and Control (CDC), 2015 IEEE 54th Annual Conference on. IEEE, 2015.

[16] Sanchez-Gasca, Juan J., and Joe H. Chow. “Power system reduction to simplify the design of damping controllers for interarea oscillations." *Power Systems, IEEE Transactions on* 11.3 (1996): 1342-1349.

[17] Nabavi, Sheida, and Aranya Chakrabortty. “Topology identification for dynamic equivalent models of large power system networks." American Control Conference (ACC), 2013. IEEE, 2013.

[18] Valdez, Justin, et al. “Fast fault location in power transmission networks using transient signatures from sparsely-placed synchrophasors." North American Power Symposium (NAPS), 2014. IEEE, 2014.
[19] Chow, Joe H., et al. “Inertial and slow coherency aggregation algorithms for power system dynamic model reduction." *Power Systems, IEEE Transactions on* 10.2 (1995): 680-685.
[20] Sanchez-Gasca, Juan J., and Joe H. Chow. “Power system reduction to simplify the design of damping controllers for interarea oscillations." *Power Systems, IEEE Transactions on* 11.3 (1996): 1342-1349.
[21] Dorfler, Florian, Michael Chertkov, and Francesco Bullo. “Synchronization in complex oscillator networks and smart grids." *Proceedings of the National Academy of Sciences* 110.6 (2013): 2005-2010.
[22] Sannuti, Peddapullaiah, and Ali Saberi. “Special coordinate basis for multivariable linear systems-finite and infinite zero structure, squaring down and decoupling." *International Journal of Control* 45.5 (1987): 1655-1704.
[23] Ishizaki, Takayuki, et al. “Model reduction of multi-input dynamical networks based on clusterwise controllability." American Control Conference (ACC), 2012. IEEE, 2012.
[24] K. Koorehdavoudi et al, “Input-Output Properties of the Swing Dynamics for Power Transmission Networks with HVDC Modulation (extended version with proofs),” available at www.eecs.wsu.edu/~kkoorehd
[25] Chen,B.M., Lin, Z., Shamash,Y. “Linear systems theory: A structural decomposition approach." Boston: BirkhÂ¨auser, 2004.
[26] P. Kundur, “Power System Stability and Control." McGraw-Hill, Inc., New York, 1994.
[27] Guoping Liu, Quintero, J.. “Oscillation monitoring system based on wide area synchrophasors in power systems." 2007 iREP Symposium Aug. 2007, pp:1- 13.
[28] C. Osauskas and A. Wood, “Small-signal dynamic modeling of HVDC systems,â€• IEEE Trans. Power Del., vol. 18, no. 1, pp. 220â€“225, Jan. 2003.
[29] D. Roberson and J. F. O’Brien, "Loop Shaping of a Wide-Area Damping Controller Using HVDC," in IEEE Transactions on Power Systems, vol. 32, no. 3, pp. 2354-2361, May 2017.
[30] J. Ma, Z. Y. Dong and P. Zhang, "Comparison of BR and QR Eigenvalue Algorithms for Power System Small Signal Stability Analysis," in IEEE Transactions on Power Systems, vol. 21, no. 4, pp. 1848-1855, Nov. 2006.
[31] Z. Du, W. Liu and W. Fang, "Calculation of rightmost eigenvalues in power systems using the Jacobi-Davidson method," in IEEE Transactions on Power Systems, vol. 21, no. 1, pp. 234-239, Feb. 2006.
[32] Schrader, Cheryl B., and Michael K. Sain. "Research on system zeros: a survey." International Journal of control 50, no. 4 (1989): 1407-1433.
[33] Hoagg, Jesse B., and Dennis S. Bernstein. "Nonminimum-phase zeros-much to do about nothing-classical control-revisited part II." IEEE control Systems 27, no. 3 (2007): 45-57.
[34] L. Zhang, H. P. Nee and L. Harnefors, "Analysis of Stability Limitations of a VSC-HVDC Link Using Power-Synchronization Control," in IEEE Transactions on Power Systems, vol. 26, no. 3, pp. 1326-1337, Aug. 2011.
[35] N. Martins, H. J. C. P. Pinto and L. T. G. Lima, "Efficient methods for finding transfer function zeros of power systems," in IEEE Transactions on Power Systems, vol. 7, no. 3, pp. 1350-1361, Aug 1992.

[36] N. Martins, P. C. Pellanda and J. Rommes, "Computation of Transfer Function Dominant Zeros With Applications to Oscillation Damping Control of Large Power Systems," in IEEE Transactions on Power Systems, vol. 22, no. 4, pp. 1657-1664, Nov. 2007.
[37] J. F. Hauer, "Robust damping controls for large power systems," in IEEE Control Systems Magazine, vol. 9, no. 1, pp. 12-18, Jan. 1989.
[38] M. M. Farsangi, Y. H. Song and K. Y. Lee, "Choice of FACTS device control inputs for damping interarea oscillations," in IEEE Transactions on Power Systems, vol. 19, no. 2, pp. 1135-1143, May 2004.
[39] M. M. Farsangi, H. Nezamabadi-pour, Y. H. Song and K. Y. Lee, "Placement of SVCs and Selection of Stabilizing Signals in Power Systems," in IEEE Transactions on Power Systems, vol. 22, no. 3, pp. 1061-1071, Aug. 2007.
[40] K. Koorehdavoudi et al., "Input-output characteristics of the power transmission network's swing dynamics," 2016 IEEE 55th Conference on Decision and Control (CDC), Las Vegas, NV, 2016, pp. 1846-1852.
[41] K. Koorehdavoudi et al., "Input-output properties of the swing dynamics for power transmission networks with HVDC modulation," to appear in Proceedings of the 20th IFAC World Congress, 2017.
[42] Small Signal Analysis Tool (SSAT), User's Manual, Powertech Labs Inc., Surrey, BC, Canada, 2002.
[43] P. Kundur, Power System Stability and Control, McGraw-Hill, 1994.
[44] Misra, Pradeep, Paul Van Dooren, and Andras Varga. "Computation of structural invariants of generalized state-space systems." Automatica 30.12 (1994): 1921-1936.
[45] E. V. Larsen and D. A. Swann, "Applying Power System Stabilizers Part I: General Concepts," in IEEE Transactions on Power Apparatus and Systems, vol. PAS-100, no. 6, pp. 3017-3024, June 1981.
[46] E. V. Larsen and D. A. Swann, "Applying Power System Stabilizers Part II: Performance Objectives and Tuning Concepts," in IEEE Transactions on Power Apparatus and Systems, vol. PAS-100, no. 6, pp. 3025-3033, June 1981.
[47] E. V. Larsen and D. A. Swann, "Applying Power System Stabilizers Part III: Practical Considerations," in IEEE Transactions on Power Apparatus and Systems, vol. PAS-100, no. 6, pp. 3034-3046, June 1981.
[48] N. Noroozian and G. Andersson, "Damping of inter-area and local modes by use of controllable components," in IEEE Transactions on Power Delivery, vol. 10, no. 4, pp. 2007-2012, Oct 1995.
[49] J. P. Corriou, Process Control: Theory and Applications, Springer, 2004.